
Dissertation
zur Erlangung des Doktorgrades
der Naturwissenschaften

der Fakultät für Biologie der
Ludwig-Maximilians-Universität München

**Correlated plasticity of synaptic structures and its
relationship to the stabilization of synaptic enlargement**



vorgelegt von
Daniel Meyer
München, 24. Januar 2013

Dissertation
zur Erlangung des Doktorgrades
der Naturwissenschaften

der Fakultät für Biologie der
Ludwig-Maximilians-Universität München

**Correlated plasticity of synaptic structures and its
relationship to the stabilization of synaptic enlargement**

vorgelegt von
Daniel Meyer
München, 24. Januar 2013

Erstgutachter: Prof. Dr. Tobias Bonhoeffer
Zweitgutachter: Prof. Dr. Rainer Uhl
Datum der Abgabe: 24. Januar 2013
Tag der mündlichen Prüfung: 18. März 2013

Die vorliegende Arbeit wurde zwischen Juni 2008 und Januar 2013 am
Max-Planck-Institut für Neurobiologie in Martinsried durchgeführt.

To my beloved family

Eidesstattliche Erklärung:

Ich erkläre hiermit an Eides statt, dass ich die Dissertation mit dem Titel "Correlated plasticity of synaptic structures and its relationship to the stabilization of synaptic enlargement" selbständig und ohne unerlaubte Beihilfe angefertigt habe. Ich habe mich dabei keiner anderen als der von mir ausdrücklich bezeichneten Hilfen und Quellen bedient.

Erklärung:

Hiermit erkläre ich, dass ich mich nicht anderweitig einer Doktorprüfung ohne Erfolg unterzogen habe. Die Dissertation wurde in ihrer jetzigen oder ähnlichen Form bei keiner anderen Hochschule eingereicht und hat noch keinen sonstigen Prüfungszwecken gedient.

München, 24. Januar 2013

Daniel Meyer

Contents

Contents	1
List of Figures	5
Abbreviations.....	7
1. Summary.....	9
2. Introduction	11
2.1 Synaptic plasticity in the hippocampus.....	11
2.2 The organization of synapses.....	12
2.3 The correlation between pre- and postsynaptic morphology.....	14
2.4 PSD-95 and Homer1c	15
2.5 NMDA receptor dependent plasticity.....	16
2.6 Structural plasticity on the level of single spines.....	18
2.7 Forskolin and the stabilization of structural modifications during single spine plasticity	19
2.8 The correlation between pre- and postsynaptic morphology during synaptic plasticity	21
2.9 Maintenance of structural and functional changes after plasticity.....	22
2.10 Objectives of this study.....	23
3. Material and Methods.....	25
3.1 Material.....	25
3.1.1 DNA constructs	25
3.1.2 Chemicals	25
3.1.3 Media and special solutions.....	26
3.1.4 Other material / equipment	27
3.2 Methods.....	28
3.2.1 Preparation of hippocampal slice cultures	28
3.2.2 Biolistic transfection of hippocampal CA1 cells	29
3.2.3 The principle of two-photon fluorescence laser scanning microscopy (TPLSM).....	29
3.2.4 The principle of glutamate uncaging	30
3.2.5 Combination of two-photon time-lapse imaging and glutamate uncaging.....	31
3.2.6 Forskolin application.....	33

3.2.7 Near infrared branding (NIRB)	33
3.7.8 Electron microscopy	34
3.2.9 Image analysis	35
3.2.10 Data analysis	36
4. Results	37
4.1 Expression of PSD-95 and Homer1c as structural marker proteins of the PSD.....	37
4.1.1 Overexpression of PSD-95 and Homer1c does not have a dramatic effect on spine volume and plasticity induction	37
4.1.2 Spine volume and PSD marker protein level correlate under naïve conditions.....	38
4.2 Plasticity induction leads to increase in spine volume and PSD marker proteins.....	40
4.2.1 Spine volume and the amount of PSD scaffolding proteins increase within one hour after spine stimulation.....	40
4.2.2 Over a period of 3 hours spine volume and PSD size move towards a new balance at a larger overall size	42
4.2.3 The correlation between spine volume and PSD-95 / Homer1c level is maintained	44
4.3 Stabilization of structural changes.....	48
4.3.1 Stabilization of structural changes goes in hand with the maintenance of the correlation between spine and PSD size	48
4.3.2 Detailed analysis of the time course of changes in PSD size and spine volume for spines with and without volume stabilization	49
4.4 Forskolin application to promote L-LTP and PSD-95 increase	50
4.5 Electron microscopy of synaptic structures after plasticity induction in spines	53
4.5.1 Electron microscopy experiments.....	53
4.5.2 Spine, PSD and bouton size correlate 3 hours after stimulation	55
5. Discussion.....	59
5.1 PSD-95 and Homer1c are appropriate marker proteins for the PSD	60
5.2 Correlation of PSD marker proteins with spine volume under naïve conditions	61
5.3 Increase of PSD marker proteins along with spine volume during plasticity	62
5.4 Reestablishment of the correlation between PSD size and spine volume	63

5.5 Stabilization of structural modifications	64
5.6 Forskolin and the stabilization of structural modifications	65
5.7 Correlation of spine, PSD and bouton size in EM reconstructions	65
6. Conclusions and Outlook	69
7. References	71
8. Acknowledgements	83
9. Curriculum Vitae	85

List of Figures

Figure 2.1: Schematic drawing of the transversal hippocampal cross section.....	12
Figure 2.2: Structure of a typical excitatory synapse.	13
Figure 2.3: Synaptic structures correlate in size.....	14
Figure 2.4: Overview of the molecular interactions in a typical excitatory synapse.	15
Figure 2.5: The neurotransmitter glutamate activates AMPA and NMDA receptors, thereby inducing synaptic plasticity.	17
Figure 2.6: Effect of forskolin on L-LTP expression and stabilization.	20
Figure 2.7: Hypothetical model of structural synaptic plasticity.	24
Figure 3.1: Principle of two-photon excitation microscopy.	30
Figure 3.2: Principle of two-photon glutamate uncaging.....	31
Figure 3.3: Schematic drawing of the optical setup used for imaging and glutamate uncaging.....	32
Figure 3.4: Scheme illustrating the pattern of the branding produced by NIRB.....	34
Figure 4.1: Labelling of spine and PSD proteins.	37
Figure 4.2: Overexpression of PSD-95-EGFP and EGFP-Homer1c does not have a dramatic effect on the volume of naïve spines and spine enlargement during structural plasticity.	38
Figure 4.3: Correlation between spine volume and PSD size in naïve spines.	39
Figure 4.4: Examples for a typical PSD-95 and Homer1c experiment.	41
Figure 4.5: Glutamate uncaging induced increase in spine volume and in the amount of PSD scaffolding proteins over 1 hour.....	42
Figure 4.6: Glutamate uncaging induced increase in spine volume and in the amount of PSD scaffolding proteins over 3 hours.	44
Figure 4.7: Time course of the PSD-volume relationship after plasticity induction.	47
Figure 4.8: The volume-PSD correlation is maintained.	48
Figure 4.9: Stability of structural changes and the relationship to PSD size.	49
Figure 4.10: Time course of PSD size and spine volume changes for spines with and without stabilized enlargement.	50
Figure 4.11: Forskolin does not have an effect on spine growth stabilization or on the increase in PSD-95 level after spine stimulation by glutamate uncaging.....	52
Figure 4.12: Electron microscopy of stimulated spines.....	54
Figure 4.13: Relationship between EM spine volume and spine fluorescence in 2-photon microscopy.	54
Figure 4.14: Characteristics of SSB and MSB synaptic contacts.	55
Figure 4.15: Electron microscopy of potentiated spines confirms PSD increase and reveals increase of bouton volume.	57

Figure 6.1: Final model illustrating the relationship between the stabilization of synapse enlargement during structural plasticity and the correlation in the dimensions of synaptic structures. 70

Abbreviations

ACSF	artificial cerebrospinal fluid
AMPA	α -amino-3-hydroxy-5-methyl-4-isoxazole propionic acid
a.u.	arbitrary units
AZ	active zone
BDMA	benzyl dimethylamine
BDNF	brain derived neurotrophic factor
CA1-CA4	cornu ammonis 1-4
CAM	cell adhesion molecule
CaMKII	Calcium / Calmodulin dependent kinase II
cAMP	cyclic adenosine monophosphate
CASK	Calcium/calmodulin-dependent serine protein kinase
CMV	cytomegalovirus
ctrl	control
DDSA	dodecenylsuccinic acid anhydride
DG	dentate gyrus
DIV	day in vitro
EC	entorhinal cortex
EGFP	enhanced green fluorescent protein
E-LTP	early long term potentiation
EM	electron microscopy
EVH1	ENA/VASP Homology 1
GK	guanylate kinase
GluR1	glutamate receptor subunit 1
LPM	litre per minute
LTD	long term depression
LTP	long term potentiation
L-LTP	late long term potentiation
mGluR	metabotropic glutamate receptor
MNA	methyl nadic anhydride
MNI-caged-L-glutamate	4-methoxy-7-nitroindolyl-caged-L-glutamate
MSB	multi-synapse bouton
NIRB	near infrared branding

NMDA	N-methyl-D-aspartate
norm.	normalized
P	postnatal day
p-value	probability value
PDZ	PSD-95, discs large, zona occludens 1
PKA	protein kinase A
PKC	protein kinase C
PSD	postsynaptic density
PSD-95	postsynaptic density protein 95
PSI	pounds per square inch
PVP	polyvinylpyrrolidone
R	correlation coefficient
Rho GTPases	Ras homolog guanosine triphosphatases
ROI	region of interest
SEM	standard error of the mean
SH3	Src homology 3 domain
SSB	single-synapse bouton
STDP	spike timing dependent plasticity
stim	stimulated
Sub	subiculum
TARP	transmembrane AMPA regulatory protein
tdTomato	tandem dimer Tomato
TPLSM	two-photon laser scanning microscopy
Tris	trihydroxymethylaminomethane
TTX	tetrodotoxin
vs.	versus

1. Summary

The ability to adapt to environmental changes, to learn and to memorize information is one of the brain's most extraordinary features. One important process underlying this ability is considered to be synaptic plasticity, i.e. the structural and functional modification of synaptic connections. Synaptic plasticity can occur either by genesis or elimination of synaptic connections, or at existing connections by modifications in the strength of synaptic transmission.

Synaptic connections are complex entities consisting of different functional structures: The majority of hippocampal and cortical excitatory synapses are made up of a postsynaptic compartment called dendritic spine and a presynaptic compartment called bouton. Within the spine and the bouton dense molecular structures, which serve the synaptic transmission between pre- and postsynapse, exist, namely the postsynaptic density (PSD) in the spine, and the active zone (AZ) in the bouton. All these structures are correlated in size and with synaptic strength. The function of this correlation serves the efficient and fast transmission of neuronal signals. During synaptic plasticity, a coordinated change in the size of all synaptic structures is expected, for the maintenance of their correlation. However, to date, such coordinated modifications have not been examined in detail. Furthermore, the mechanisms underlying the maintenance of structural and functional changes after synaptic plasticity remain poorly understood. The aim of this thesis was to explore these questions. To achieve this I carried out two complementing experimental approaches:

In a first set of experiments, I studied changes in spine and PSD size by two-photon time-lapse imaging to explore correlated modifications in these two synaptic structures. To induce structural spine plasticity I stimulated single dendritic spines of Schaffer collateral synapses in cultured hippocampal slices by two-photon glutamate uncaging. This was shown previously to be accompanied by an increase in spine size and synaptic strength. To visualize structural plasticity of spines and their PSD, the cytosolic marker tdTomato and EGFP-tagged structural proteins of the PSD, namely PSD-95 and Homer1c, were co-expressed. PSD-95 and Homer1c are important and abundant scaffolding proteins of the PSD, which have been used previously as markers for PSD size. I found that both PSD-95 and Homer1c levels increased after spine stimulation. Homer1c increased rather rapidly whereas PSD-95 did so in a delayed manner relative to the increase in spine volume. Thus, the naïve correlation between PSD protein level and spine

volume was only transiently disrupted after plasticity induction, but was reestablished over a time course of 3 hours. Furthermore, PSD-95 level only increased significantly in spines with persistent enlargement, but not in spines with non-persistent enlargement. On the other hand, Homer1c level initially increased both in spines with and without persistent enlargement, and then decayed back to original level in spines with non-persistent enlargement. Because the increase in PSD-95 level was delayed, I investigated whether the application of the PKA activator forskolin, which supports an increased and persistent enlargement of spines after glutamate uncaging, might promote and therefore accelerate an increase in PSD-95 level. However, these experiments led to unexpected results: forskolin application neither had an effect on spine volume nor on PSD-95 level increase.

Although PSD-95 and Homer1c are important and abundant PSD scaffolding proteins, they represent only two out of a multitude of proteins which form the PSD. Consequently, an increase in the PSD marker proteins does not necessarily represent an increase of the PSD as a whole. Therefore, in a second experimental approach, I applied electron microscopy to stimulated spines which displayed a stable enlargement over 3 hours after stimulation. Hereby, I was able not only to reconstruct the spine and the entire PSD, but also the bouton at the stimulated spine: I found that spine, PSD and bouton displayed matching dimensions 3 hours after stimulation, similar to naïve, unstimulated spines.

In summary, by combining two-photon glutamate uncaging with time-lapse imaging and electron microscopy, I found that spine, the PSD and bouton increase during structural plasticity, and that the correlation between these structures is reestablished after stimulation on a time scale of 3 hours. Furthermore, an increase of synaptic structures correlates with the stabilization of synaptic modifications after plasticity. This suggests a model where the balancing of synaptic structures is a hallmark for the stabilization of structural modifications during synaptic plasticity.

2. Introduction

2.1 Synaptic plasticity in the hippocampus

In neuroscience, plasticity is defined as the ability of neuronal structures to undergo morphological and functional changes in order to adapt to stimuli or environmental alterations. Synaptic plasticity in particular describes a change in the connectivity of neurons or in the strength of synaptic transmission, and is an activity dependent process as first postulated by Donald O. Hebb (Hebb, 1949). It is considered to be the cellular basis for learning and memory.

In general, two forms of long-term synaptic plasticity exist: long-term potentiation (LTP) and long-term depression (LTD), leading to a persistent increase or decrease in synaptic strength, respectively (Malenka et al., 2004). First experimental evidence for LTP came from Bliss and Lomo, by demonstrating that brief, repetitive activation of excitatory synapses leads to long-term enhancement of synaptic strength (Bliss et al., 1973). Various forms of LTP and LTD exist (Malenka et al., 2004; Castillo, 2012), differing from each other in the molecular mechanisms leading to their establishment. The most prominent form of LTP in glutamatergic synapses of the cortex is referred to as NMDA receptor dependent LTP (Luscher et al., 2012), which is the form of LTP which I will focus on in my thesis. It will be described in more detail in section 2.5.

Because the induction of NMDA receptor dependent LTP is well established at the Schaffer collateral synapse in the CA1 region of the hippocampus (Malenka et al., 1993; Malenka et al., 2004) (Figure 2.1), I explicitly studied these synapses during my experiments. In general, owing to its well-arranged structure and its importance for learning and memory, the hippocampus has become a prominent brain structure widely used for studying synaptic plasticity.

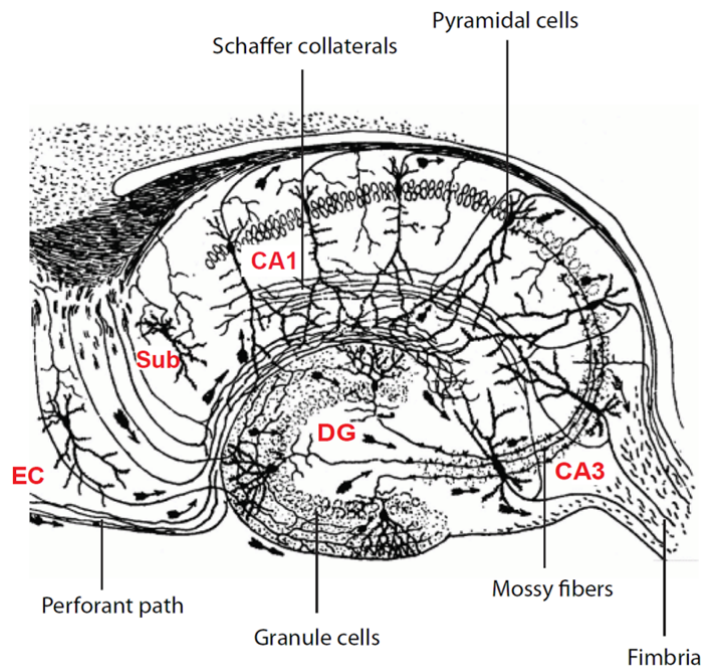


Figure 2.1: Schematic drawing of the transversal hippocampal cross section.

The classical circuit within the hippocampus is as follows (Squire et al., 1991): input from the entorhinal cortex (EC) arrives via the perforant path at granule cells of the dentate gyrus (DG). Signals are then forwarded via mossy fibers to the CA3 region and then via Schaffer collaterals to pyramidal cells of the CA1 area. Finally, information leaves the hippocampus via the subiculum (Sub) back into the EC. Modified from Cajal, 1911.

2.2 The organization of synapses

Synapses are specialized connections between neurons, enabling them to communicate with each other. On each neuron, several thousand synapses are located. With respect to the direction of signal transmission between neurons, synapses consist of a presynaptic and a postsynaptic specialization, which are separated by the synaptic cleft.

Most presynaptic specializations are located on the axons of a nerve cell, in the form of so called boutons. The bouton contains synaptic vesicles filled with neurotransmitter. Opposed to the presynapse, the postsynapse resides. It contains the receptors for the neurotransmitter released from the bouton, thereby constituting the signal receiving unit of the postsynaptic cell. Postsynapses are located on dendrites. Dendrites integrate and conduct synaptic signals to their neuron's cell body, where a new signal in the form of an action potential can be produced.

In pyramidal neurons, about 80% of postsynapses appear on small protrusions originating from the dendrites, which are therefore called dendritic spines (Nimchinsky et al., 2002). Spines have different functions: first, they serve as substrate for synapse formation by bridging the gap between axons and dendrites. Second, they contain the molecular signalling complexes controlling synaptic strength (Kim et al., 2004; Newpher et al., 2009) and compartmentalize chemical signals such as calcium, which is a key player in synaptic plasticity (Hering et al., 2001; Chen et al., 2012).

Spines can have different shapes, ranging from “stubby” spines over “mushroom-like” spines to “thin” spines, having a “long neck and small head” (Peters et al., 1970; Yuste et al., 2004; Yoshihara et al., 2009). Previous studies suggest that filopodia-like protrusions and spines with long necks and small heads represent developing spines, whereas mushroom-like spines are considered as mature and functional postsynaptic structures (Yuste et al., 2004; Lohmann et al., 2008; Yoshihara et al., 2009). The role of stubby spines is less clear. They probably can represent both, developing or functional spines.

Synapses exhibit specific dense molecular structures close to the synaptic cleft, both on the presynaptic and postsynaptic site, respectively (Figure 2.2).

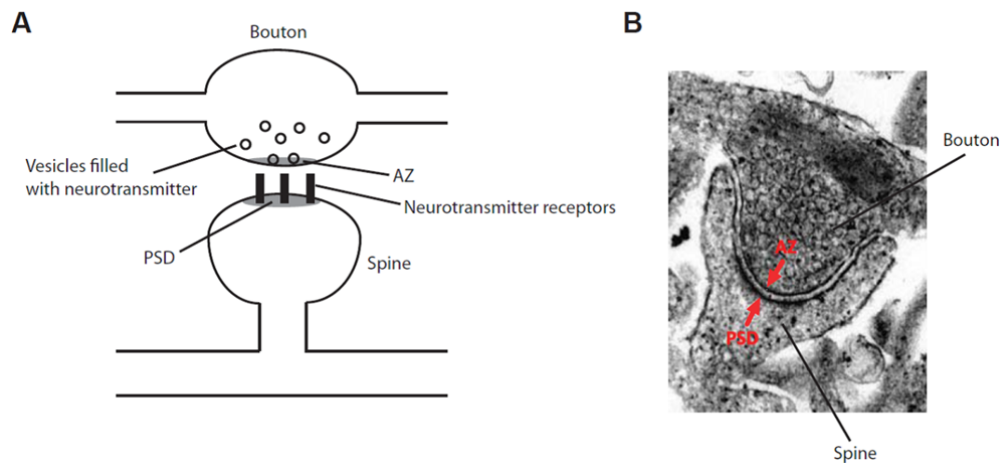


Figure 2.2: Structure of a typical excitatory synapse.

(A) Schematic drawing of presynaptic bouton and postsynaptic spine. From boutons neurotransmitter is released at the active zone by fusion of neurotransmitter-containing vesicles with the presynaptic membrane. On the postsynaptic site specific receptors are located in the PSD, which are activated by the neurotransmitter.

(B) Electron micrograph of a synapse, showing a bouton contacting a dendritic spine. The black structures at the pre- and postsynaptic membranes represent the AZ and PSD, respectively (marked by red arrows). Both are closely aligned to each other.

On the presynaptic site this structure is called the active zone (AZ) (Schoch et al., 2006; Harris et al., 2012). Here neurotransmitter is released into the synaptic cleft by fusion of neurotransmitter-containing vesicles with the synaptic membrane. On the postsynaptic site the dense molecular structure is called the postsynaptic density (PSD). It contains the receptors to which the released neurotransmitter binds (Sheng et al., 2007; Harris et al., 2012). The AZ is closely and precisely aligned with the PSD (Schikorski et al., 1997) (Figure 2.2).

2.3 The correlation between pre- and postsynaptic morphology

It was demonstrated by electron microscopy that at excitatory synapses of pyramidal neurons in the cortex and hippocampus the size of the structural elements of synapses (presynaptic bouton, the pool of synaptic vesicles, the AZ, the PSD and postsynaptic spine head volume) are correlated (Harris et al., 1989; Schikorski et al., 1999; Arellano et al., 2007) (Figure 2.3). This correlation of synaptic structures and the alignment between AZ and PSD is thought to increase the speed and efficacy of chemical synaptic transmission.

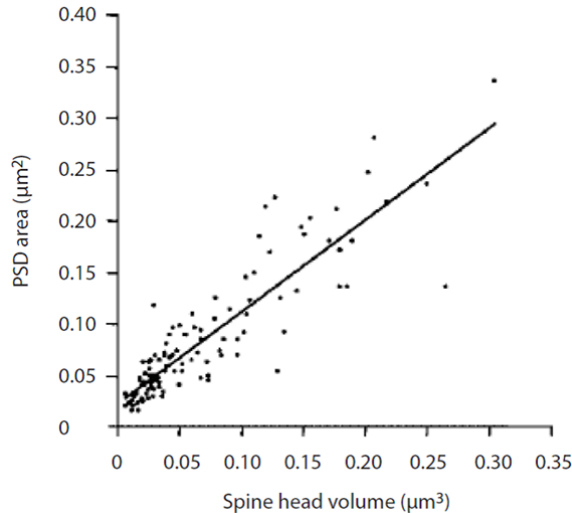


Figure 2.3: Synaptic structures correlate in size.

Correlation between PSD size and spine volume as example for the general correlation between synaptic structures. Data were obtained by electron microscopy. Adapted from Arellano et al., 2007.

Furthermore, the size of the presynaptic vesicle pool, the amount of neurotransmitter release and the number of neurotransmitter receptors correlate with synaptic strength. Therefore the size of the bouton, AZ, PSD and

spine should be a direct measure for synaptic strength (Bredt et al., 2003; Schoch et al., 2006; Sheng et al., 2007). Indeed, it was found that the strength of synaptic transmission is correlated with the size of all these synaptic structures (e.g. Takumi et al., 1999; Matsuzaki et al., 2001; Murthy et al., 2001; Holderith et al., 2012).

2.4 PSD-95 and Homer1c

Both, the PSD and AZ consist of a multitude of synaptic proteins, for the PSD see Figure 2.4. Among them so called scaffolding proteins form a molecular network structure at which specific proteins such as glutamate receptors, signalling molecules and transport proteins are assembled into large molecular complexes (Kim et al., 2004).

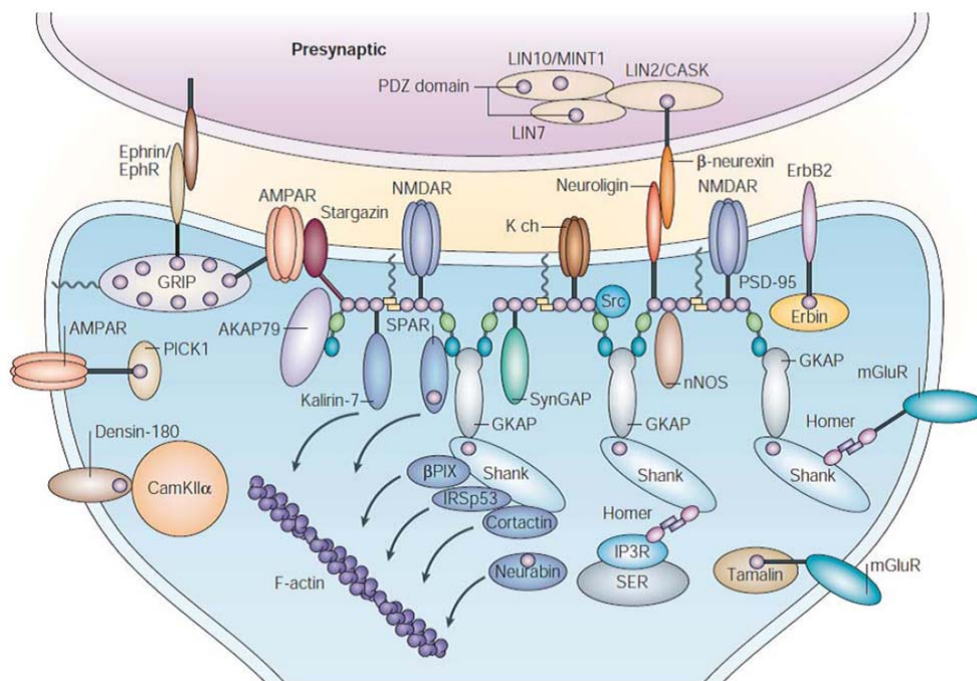


Figure 2.4: Overview of the molecular interactions in a typical excitatory synapse.

The synapse contains a multitude of proteins. Here a subset of the most relevant postsynaptic proteins is shown. Synaptic proteins can be classified according to their function, e.g. into scaffolding proteins of the PSD like PSD-95 and Homer1c, cell adhesion molecules like Neuroigin / Neurexin which potentially mediate coordinated plasticity, cytoskeletal proteins like actin which regulates changes in spine morphology, signalling molecules like CaMKII which regulates synaptic processes such as plasticity, and receptor ion channels like AMPA and NMDA receptors which determine synaptic strength and regulate plasticity. Adapted from Kim et al., 2004.

Two of the most important scaffolding proteins of the PSD are PSD-95 and Homer1. Both are often used as markers for the PSD and tagged with fluorescent proteins (Gray et al., 2006; Steiner et al., 2008; Petrini et al., 2009). PSD-95 belongs to the family of PDZ proteins, a large group of multi-domain scaffolding proteins (the name refers to the proteins in which the PDZ domain was originally identified: PSD-95, discs large, zona occludens 1) (Kim et al., 2004). PSD-95 contains three of such PDZ domains, one SH3 (Src homology 3 domain) and one GK (guanylate kinase-like) domain. All these domains are protein-protein interaction domains. PSD-95 is located close to the postsynaptic membrane and directly interacts with NMDA receptors, as well as indirectly with AMPA receptors via stargazin, a transmembrane AMPA regulatory protein (TARP) (Sheng et al., 2001; Valtschanoff et al., 2001; Kim et al., 2004; Nicoll et al., 2006; Chen et al., 2008). Therefore, PSD-95 serves as an important scaffold for anchoring glutamate receptors, hereby regulating synaptic strength and synaptic plasticity (El-Husseini et al., 2000; Beique et al., 2003; Ehrlich et al., 2004; Ehrlich et al., 2007; Chen et al., 2011).

In contrast to PSD-95, Homer1 is located at the cytoplasmic face of the postsynapse. Three splice variants of Homer1 exist: Homer1a is a short form of Homer which is monomeric and exhibits only an EVH1 domain (ENA/VASP Homology 1 domain). In contrast Homer1b and Homer1c are long forms, tetrameric and have both an EVH1 as well as a coiled coil domain. The coiled coil domain is involved in self-association of the protein (Hayashi et al., 2006; Shiraishi-Yamaguchi et al., 2007; Hayashi et al., 2009). Homer interacts with the scaffolding protein Shank to form a polymeric network structure, and it binds directly to metabotropic glutamate receptors (mGluRs), which regulate postsynaptic responses (Cosgrove et al., 2011).

2.5 NMDA receptor dependent plasticity

In section 2.1 NMDA receptor dependent plasticity was introduced as a prominent and well-studied form of plasticity. Here I will describe it in more detail. In NMDA receptor dependent plasticity so called AMPA (α -amino-3-hydroxy-5-methyl-4-isoxazole propionic acid) and NMDA (N-methyl-D-aspartat) receptors play a crucial role. AMPA receptors mediate postsynaptic depolarization and therefore synaptic transmission. NMDA receptors also contribute to depolarization, but in addition initiate synaptic plasticity (Luscher et

al., 2012): The AMPA receptor mediated depolarization through Na^+ influx results in the removal of the Mg^{2+} block from NMDA receptors, which allows ions, such as Na^+ and Ca^{2+} , to pass when the receptors are activated by glutamate (Figure 2.5 A). Ca^{2+} then activates various signalling cascades involved in spine plasticity.

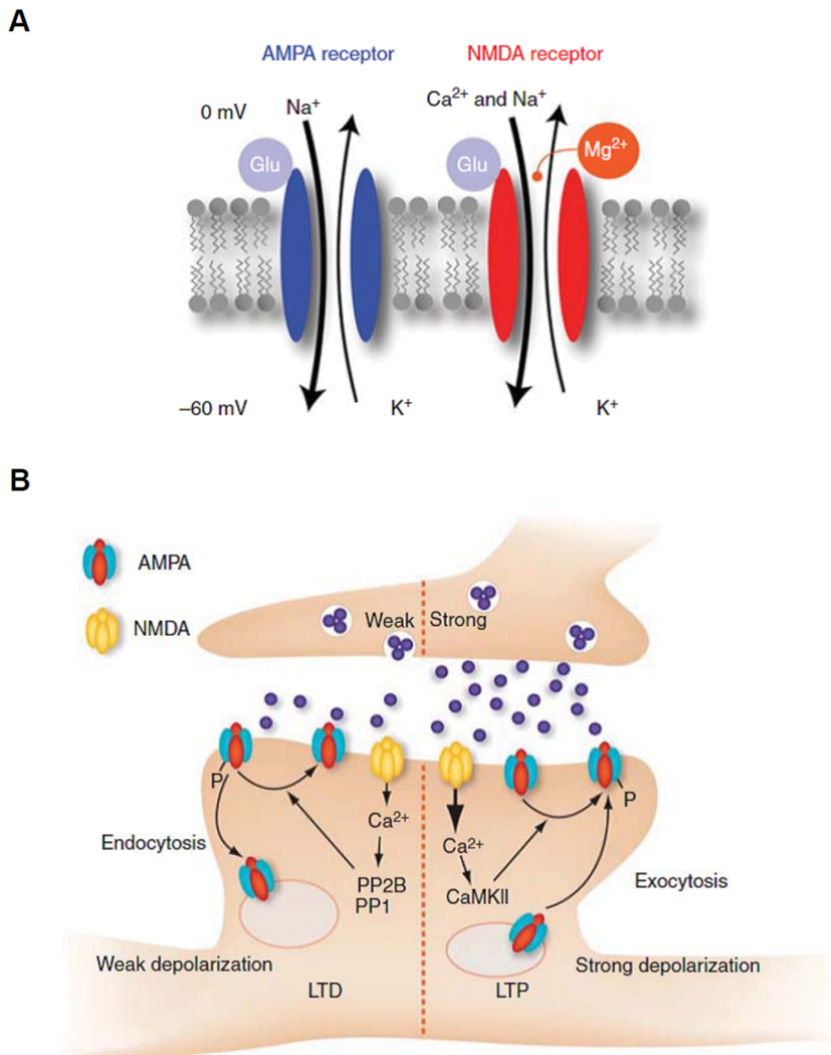


Figure 2.5: The neurotransmitter glutamate activates AMPA and NMDA receptors, thereby inducing synaptic plasticity.

(A) Binding of glutamate to AMPA receptors leads to Na^+ influx. As a consequence the postsynapse is depolarized. If the depolarization is strong enough, Mg^{2+} is expelled from activated NMDA receptors, allowing Ca^{2+} influx.

(B) Weak neurotransmitter release is accompanied by low Ca^{2+} influx, leading to the activation of phosphatases and LTD. In contrast, strong neurotransmitter release results in strong Ca^{2+} influx, leading to the activation of kinases and LTP. Noteworthy, the strength of Ca^{2+} influx is not only determined by the amount of neurotransmitter but also by other factors such as spike timing (not shown here). Adapted from Luscher et al., 2012.

Particularly important, while weak Ca^{2+} influx activates phosphatases, leading to LTD (Luscher et al., 2012), strong Ca^{2+} influx activates kinases, for example PKC (protein kinase C) and CaMKII (Ca^{2+} / calmodulin dependent protein kinase II) (Luscher et al., 2012), and leads to LTP (Figure 2.5 B). The activated kinases result in the insertion of additional AMPA receptors into the synaptic membrane, as well as in an increased conductance of AMPA receptors. This leads to strengthening of signal transmission and therefore to LTP (Bredt et al., 2003; Malinow, 2003; Luscher et al., 2012) (Figure 2.5 B). Ca^{2+} influx is strong if the postsynaptic neuron is sufficiently depolarized during presynaptic neurotransmitter release, i.e. when many NMDA receptors are free from blockage by Mg^{2+} . Under physiological conditions this for example occurs during spike timing dependent plasticity (STDP), i.e. when back propagating action potentials reach the postsynapse shortly after the presynapse released neurotransmitter (Luscher et al., 2012).

NMDA receptor dependent LTP can be subdivided into different temporal phases: a short fragile period, lasting about 15-30 minutes after induction, during which LTP is susceptible to reversal (Staubli et al., 1999). This phase is followed by a stage referred to as early LTP (E-LTP). E-LTP lasts for about 1 hour and is independent of protein synthesis (Redondo et al., 2011). In contrast, the last phase of long-term potentiation, late LTP (L-LTP), is characterized by its dependence on protein synthesis and persists over a long period of time (Redondo et al., 2011).

2.6 Structural plasticity on the level of single spines

Functional changes in signal transmission between the pre- and postsynapse during NMDA receptor dependent LTP also correlate with structural changes: Confocal or two-photon time-lapse imaging before and after plasticity induction on the subcellular level showed that potentiation of synaptic connections is structurally accompanied by an enlargement of preexisting dendritic spines, and formation of new spines (e.g. Hosokawa et al., 1995; Engert et al., 1999; Maletic-Savatic et al., 1999; Kopec et al., 2007). The structural plasticity of dendritic spines was shown to be based on a complex network of biochemical signalling cascades. It involves the highly dynamic actin cytoskeleton within the spine, regulating structural changes on a time scale of seconds to minutes (Okamoto et al., 2004; Honkura et al., 2008).

The studies described above involved the stimulation of many synapses, and the observed changes were not confined to a single synaptic contact. However, it is important to conduct longitudinal studies at the level of individual spines, which receive a defined stimulus for plasticity induction. This enables exploring input specific changes, which are not affected by global effects such as balancing of modifications by redistribution of synaptic weights.

Studying plasticity in single spines has first been achieved by combining time-lapse two-photon imaging with local stimulation of single spines by two-photon glutamate uncaging (see methods) (Matsuzaki et al., 2004). Hereby it has been shown that also at the level of a single stimulated synapse functional potentiation is indeed accompanied by spine enlargement, and in particular, that there is a tight correlation between synaptic strength and spine head volume (Matsuzaki et al., 2004; Harvey et al., 2007). Furthermore, Matsuzaki et al. showed that stimulating single spines by glutamate uncaging leads to persistent spine enlargement only in small spines ($< 0.1 \mu\text{m}^3$) but transient enlargement in large spines ($> 0.1 \mu\text{m}^3$). Like NMDA dependent LTP, spine enlargement induced by glutamate uncaging depends on NMDA receptors, CaMKII, Rho GTPases and actin polymerization (Matsuzaki et al., 2004; Okamoto et al., 2004; Sobczyk et al., 2005; Lee et al., 2009; Murakoshi et al., 2011). This suggests that glutamate uncaging induced plasticity is a structural correlate of functional LTP.

2.7 Forskolin and the stabilization of structural modifications during single spine plasticity

As described, LTP occurs in different temporal phases (see section 2.5). The last phase, which is referred to as L-LTP, represents the stabilization of synaptic strengthening over an extended period of time, and it depends on protein synthesis. On the molecular level, protein synthesis is induced by different signalling pathways. For example, the presence of BDNF around the time of glutamate uncaging seems to play an important role in the stabilization of spine enlargement by acting on protein synthesis (Tanaka et al., 2008). Furthermore, BDNF leads to the transport of PSD-95 into the dendrite and into dendritic spines (Yoshii et al., 2007). BDNF signalling is connected to the PKA (protein kinase A) pathway since PKA signalling results in the release of BDNF into the synaptic cleft (Kuczewski et al., 2010). Activation of the PKA pathway also leads to protein synthesis and stabilization of spine volume increase after glutamate uncaging

(Abel et al., 1997). The PKA pathway can be stimulated by application of the adenylylcyclase activator forskolin (Figure 2.6 A).

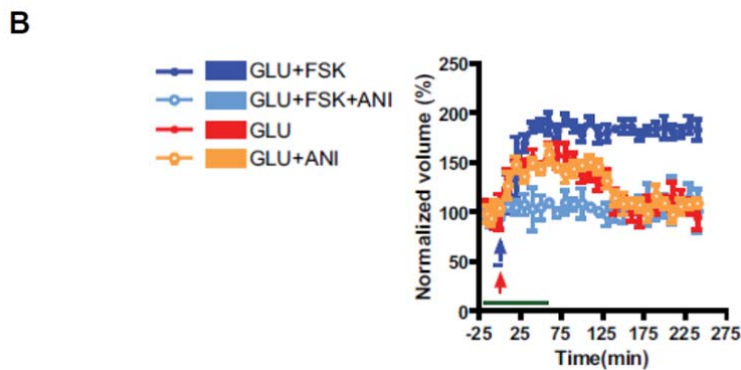
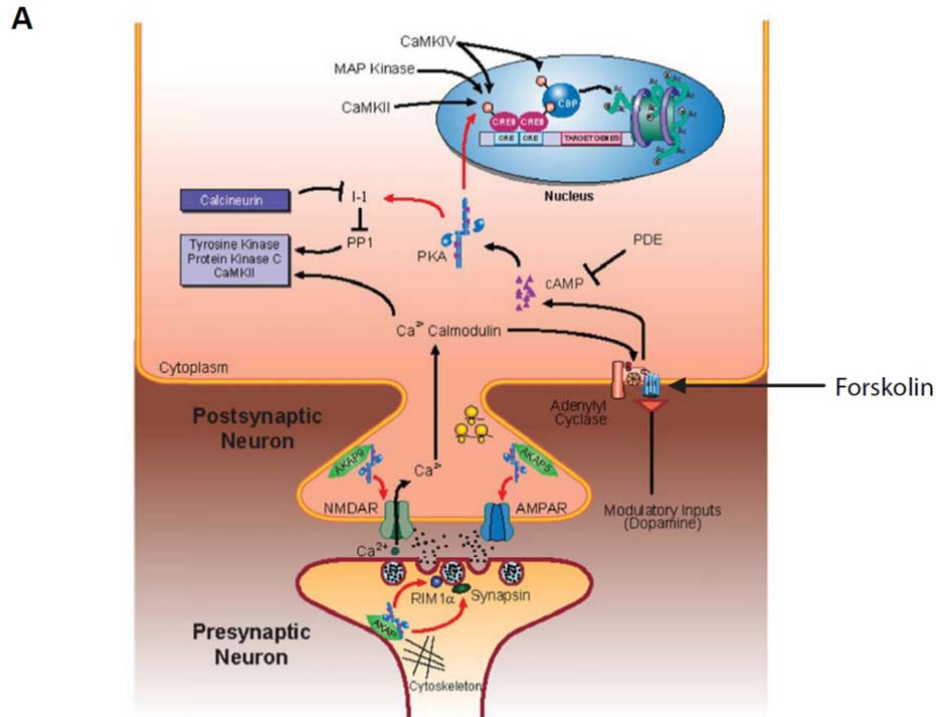


Figure 2.6: Effect of forskolin on L-LTP expression and stabilization.

(A) Forskolin positively acts on adenylylcyclase which activates the PKA pathway. This in turn leads to the activation of kinases, transcription factors and protein synthesis. As a result L-LTP is promoted. Modified from Abel et al., 2008.

(B) Forskolin supports L-LTP formation, leading to an increased enlargement of spines after glutamate uncaging and to the stabilization of the spine enlargement. Blue bar represents time interval of forskolin application (green bar: anisomycin). Blue and red arrows represent uncaging stimuli. GLU = glutamate, FSK = forskolin, ANI = anisomycin. Modified from Govindarajan et al., 2011.

Activated adenylyl cyclase leads to cAMP production, which in turn activates the PKA pathway (Frey et al., 1993; Frey et al., 1998; Abel et al., 2008). This leads to an increased spine enlargement and the stabilization of the spine volume increase over extended time, as structural correlate of L-LTP (Govindarajan et al., 2011) (Figure 2.6 B).

2.8 The correlation between pre- and postsynaptic morphology during synaptic plasticity

The correlation of synaptic structures (see section 2.3) predicts that structural spine plasticity should be accompanied by structural modifications also of the PSD as well as presynaptic AZ and bouton. So far, studies into such modifications, which applied electron microscopy to brain tissue after plasticity induction, yielded conflicting results (reviewed e.g. in Yuste et al., 2001). After LTP induction, there was in some but not all preparations (e.g. Sorra et al., 1998) an increase in the size of dendritic spines (e.g. Van Harreveld et al., 1975; Desmond et al., 1983), PSDs (e.g. Desmond et al., 1983; Desmond et al., 1986) as well as in the apposed post- and presynaptic membrane area (e.g. Desmond et al., 1988). These synaptic structural modifications were observed at the population level, i.e. as average changes of many synapses. However, at the level of individually stimulated synapses almost nothing is known about the plasticity of synaptic structures aside from the spine.

Correlated modifications of synaptic structures during plasticity would demand a coordination of the underlying molecular processes, which would most likely arise from interaction between synaptic proteins. In particular, the link between coordinated changes in spine volume and PSD size might be found in direct or indirect interactions between the spine actin cytoskeleton and the proteins of the PSD. Spine enlargement during potentiation is mediated by actin polymerization (e.g. Okamoto et al., 2004; Honkura et al., 2008), and actin cytoskeleton dynamics produces changes in PSD morphology (e.g. Blanpied et al., 2008). Actin is linked via Cortactin to the PSD scaffolding protein Shank, which in turn binds directly to Homer and via GKAP to PSD-95 (Hering et al., 2001). Moreover, Cortactin interacts with Arp2/3, an actin nucleation factor, which positively regulates actin polymerization (Weed et al., 2000). In addition PSD-95 interacts with the actin regulating protein kalirin-7 (Xie et al., 2007).

A major role in the coordination of pre- and postsynaptic plasticity might play cell adhesion molecules (CAMs): CAMs are membrane bound proteins, which contain an extracellular CAM-CAM interaction domain. Each postsynaptic CAM interacts via a CAM-CAM interaction domain with a presynaptic CAM. Hereby, CAMs link the pre- and postsynaptic compartments and might provide the transsynaptic signal which coordinates pre- and postsynaptic structural plasticity (reviewed e.g. in Dalva et al., 2007).

Among CAMs, for example Ephrins and Ephs might be involved in reverse transsynaptic signalling (Grunwald et al., 2004; Dalva et al., 2007; Egea et al., 2007). Ephrins and Ephs are located both in the pre- and postsynapse, and can interact with each other in converse, bi-directional ways. EphB2 directly binds to NMDA receptors, and is also indirectly associated with AMPAR receptors via GRIP/PICK. It has been shown that genetic ablation of EphrinB2 and EphrinB3 leads to defects in LTP (Grunwald et al., 2004).

Other candidate CAMs are N-cadherin and neuroligin / neurexin. LTP induction leads to accumulation of N-cadherin in stimulated spines (Mendez et al., 2010). Furthermore, postsynaptic overexpression of PSD scaffolding proteins including PSD-95 and SAP-97 leads to increased presynaptic protein level and presynaptic potentiation in a manner depending on N-cadherin, and also neuroligin / neurexin (El-Husseini et al., 2000; Regalado et al., 2006; Futai et al., 2007). Neuroligin is a CAM located in the postsynaptic membrane, and Neurexin is its presynaptic binding partner. Neuroligin has been shown to recruit NMDARs and AMPARs to synapses. Therefore, N-Cadherin and Neuroligin / Neurexin build at least a structural connection between post- and presynaptic plasticity.

As the postsynaptic CAMs interact with postsynaptic structural proteins so do the presynaptic CAMs with presynaptic structural and scaffolding proteins (Gundelfinger et al., 2012). Neurexin for example interacts with CASK (Ca²⁺ / calmodulin dependent serine protein kinase), a major scaffolding protein of the AZ.

2.9 Maintenance of structural and functional changes after plasticity

How are changes in synaptic strength ultimately stabilized and maintained? Structural changes themselves have been proposed to be a signature of LTP maintenance (Abraham et al., 2003). At the molecular level, a number of structural and scaffolding proteins as well as cell adhesion molecules (see above)

are involved in structural synaptic plasticity and the stabilization of LTP. At the level of individual spines, actin, PSD-95, the glutamate receptor subunit GluR1 and the CAM cadherin are implicated in the stabilization of spine volume changes (Ehrlich et al., 2007; Kopec et al., 2007; Honkura et al., 2008; Bozdagi et al., 2010; Mendez et al., 2010). With respect to functional potentiation, actin as determining factor of spine size, PSD-95 as glutamate receptor anchor in the PSD, and CAMs as candidates for structural transsynaptic signalling were suggested to play a role in the stabilization of LTP (Bozdagi et al., 2000; Krucker et al., 2000; Kramar et al., 2006; Ehrlich et al., 2007). Therefore, the molecular processes underlying the stabilization of both structural and functional modifications share a common pool of involved proteins, highlighting the strong structure-function relationship in the maintenance of plasticity related changes. Although in none of the studies described above correlated changes were shown directly, taken together, the individual examples suggest that coordinated structural plasticity promotes the maintenance and stabilization of both structural and functional changes during plasticity.

2.10 Objectives of this study

The correlation between synaptic structures suggests that during plasticity coordinated changes have to occur in these structures, leading to the reestablishment of the correlation between synaptic structures after the plasticity processes are completed. However, except for the spine, only little is known about the plasticity of synaptic structures at the level of a single synapse. Furthermore, while the processes underlying the induction of spine plasticity have been intensively studied, the mechanisms leading to the stabilization of synaptic modifications remain still elusive. In my thesis, I extended the analysis of structural plasticity at the level of individual, stimulated spines to other synaptic structures of both the post- and presynapse. In particular, I examined the following two hypotheses:

1. Along with the spine volume, other synaptic structures, in particular the PSD and presynaptic bouton, enlarge during synaptic potentiation.
2. The balancing of the synaptic structures is a signature for the stabilization of structural modifications (Figure 2.7).

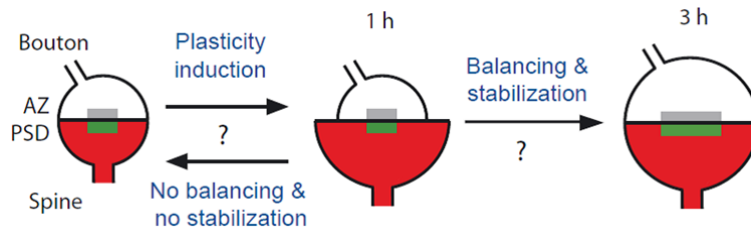


Figure 2.7: Hypothetical model of structural synaptic plasticity.

Plasticity induction leads to an increase in spine volume. Depending on whether the other synaptic structures (PSD, AZ and bouton) also increase, synaptic modifications will be ultimately stabilized or the spine returns to its original size.

In addition, I explored the time courses of the enlargement of synaptic structures. To accomplish these objectives I applied two different complementing experimental approaches:

First, I monitored in real time structural plasticity of spines and their PSDs in pyramidal cells of cultured hippocampal slices using two-photon microscopy. For this purpose I labelled the spine volume and the PSD by expressing a fluorescent cytosolic marker as well as EGFP-tagged structural proteins of the PSD. As such I chose PSD-95 and Homer1c, two abundant and important scaffolding proteins of the PSD (see section 2.4). Plasticity was induced at single spines of CA3-CA1 Schaffer collateral synapses by two-photon glutamate uncaging.

In the second approach, I reconstructed Schaffer collateral synapses by electron microscopy after spine plasticity induction, and determined spine volume, PSD size as well as presynaptic bouton volume. Thereby, I obtained information about the structural changes of the PSD as a morphological entity as well as on presynaptic structural modifications.

The two approaches showed that indeed, after spine stimulation, synaptic structures increase, and that the correlation between synaptic structures is reestablished.

3. Material and Methods

3.1 Material

3.1.1 DNA constructs

Tab. 3.1: DNA constructs used to label cell morphology and the PSD.

Construct	Promotor	Resistance	Source
pEGFP-N1	CMV	Kanamycin	Prof. Dr. Valentin Stein, Physiology Department 2, University of Bonn, Bonn, Germany
pCI-Neo PSD-95-EGFP	CMV	Ampicillin	Prof. Dr. Valentin Stein, see above
pcDNA EGFP-Homer1c	CMV	Ampicillin	Prof. Dr. Daniel Choquet, Interdisciplinary Institute for Neuroscience, Bordeaux, France; see Petrini et al., 2009
pcDNA3 tdTomato	CMV	Ampicillin	Dr. Corette Wierenga, Department of Biology, University of Utrecht, Utrecht, Netherlands

3.1.2 Chemicals

Tab. 3.2: List of chemicals and solutions used for experiments.

Chemical	Supplier
α -D(+)-Glucose•H ₂ O	Carl Roth, Karlsruhe, Germany
Ampicillin	Sigma-Aldrich, Steinheim, Germany
BDMA	Serva Electrophoresis, Heidelberg, Germany
CaCl ₂	Sigma-Aldrich, Steinheim, Germany
Carbogen (95% O ₂ , 5% CO ₂)	Westfalen AG, Münster, Germany
DBA	Serva Electrophoresis, Heidelberg, Germany
Diaminobenzidine	<i>Sigmafast 3,3'-Diaminobenzidine</i> tablets, Sigma-Aldrich, Steinheim, Germany
D-Serine	Biotrend Chemikalien, Köln, Germany
Ethanol absolute	Sigma-Aldrich, Steinheim, Germany
Forskolin	Enzo Life Sciences, Lörrach, Germany
Glutaraldehyde	Electron Microscopy Sciences, Hatfield, USA
Glycidether 100	Serva Electrophoresis, Heidelberg, Germany
HBSS	Life Technologies (Invitrogen/Gibco), Darmstadt, Germany
Helium	Westfalen AG, Münster, Germany
HEPES	Carl Roth, Karlsruhe, Germany

Chemical	Supplier
Horse serum	Life Technologies (Invitrogen/Gibco), Darmstadt, Germany
Kanamycin	Sigma-Aldrich, Steinheim, Germany
KCl	Sigma-Aldrich, Steinheim, Germany
Kynurenic acid	Sigma-Aldrich, Steinheim, Germany
Lead citrate	Leica Microsystems, Wetzlar, Germany
MEM medium	Life Technologies (Invitrogen/Gibco), Darmstadt, Germany
MNA	Serva Electrophoresis, Heidelberg, Germany
MNI-caged-L-glutamate	Tocris Bioscience, Bristol, United Kingdom
NaCl	VWR International, Leuven, Belgium
NaHCO ₃	Merck, Darmstadt, Germany
NaH ₂ PO ₄ •H ₂ O	Merck, Darmstadt, Germany
Nitrogen	Westfalen AG, Münster, Germany
Paraformaldehyde	Electron Microscopy Sciences, Hatfield, USA
Propylen oxide	Electron Microscopy Sciences, Hatfield, USA
PVP (Polyvinylpyrrolidon)	Bio-Rad, München, Germany
Sodium cacodylate buffer (pH 7.4)	Electron Microscopy Sciences, Hatfield, USA
Spermidine	Sigma-Aldrich, Taufkirchen, Germany
Sucrose	Merck, Darmstadt, Germany
Tris buffer (pH 7.4) (obtained from <i>Trizma Base</i> tablets)	Sigma-Aldrich, Munich, Germany
Trolox	Sigma-Aldrich, Taufkirchen, Germany
TTX (Tetrodotoxin)	Biotrend Chemikalien, Köln, Germany
Uranyl acetate	Leica Microsystems, Wetzlar, Germany

3.1.3 Media and special solutions

Tab. 3.3: List of media and special solutions.

Medium / Solution	Chemical	Concentration
ACSF (artificial cerebro-spinal fluid) (pH 7.2)	α-D(+)-Glucose•H ₂ O	25 mM
	CaCl ₂	4 mM
	D-Serine	10 μM
	KCl	2.5 mM
	NaCl	127 mM
	NaHCO ₃	15 mM
	NaH ₂ PO ₄ •H ₂ O	1.25 mM
	Sucrose	20 mM
	Trolox	1 mM
	TTX	1 μM
Forskolin-ACSF (pH 7.2) (for experiments with forskolin application)	100% (v/v) ACSF	
	Forskolin	50 μM
Fixative	Glutaraldehyde	2.5% (v/v)
	NaCl	154 mM
	Paraformaldehyde	2% (m/v)
	Na ₂ HPO ₄	80 mM

Medium / Solution	Chemical	Concentration
	NaH ₂ PO ₄	20 mM
MNI-caged-L-glutamate solution (pH 7.4) (for local pipette application)	α-D(+)-Glucose•H ₂ O CaCl ₂ D-Serine HEPES KCl MNI-caged-L-glutamate NaCl NaHCO ₃ NaH ₂ PO ₄ •H ₂ O TTX	25 mM 4 mM 10 μM 40 mM 2.5 mM 12 mM 118.5 mM 2 mM 1.25 mM 1 μM
Resin	Glycidether 100 + MNA Glycidether 100 + DDSA BDMA	100 mL + 89 mL 62 mL + 100 mL 6.3 mL
Slice-culture medium (pH 7.2)	α-D(+)-Glucose•H ₂ O HBSS HEPES Horse serum MEM	50 mM 25% (v/v) 25% (v/v) 12.5 mM 75% (v/v)
Slice-preparation medium (pH 7.2)	α-D(+)-Glucose•H ₂ O CaCl ₂ •2H ₂ O KH ₂ PO ₄ Kynurenic acid MgSO ₄ •7H ₂ O NaHCO ₃ KCl MgCl ₂ •6H ₂ O NaCl Na ₂ HPO ₄	55.5 mM 1.5 mM 220 μM 100 mM 284 μM 2.7 mM 5 mM 1 mM 137 mM 845 μM

3.1.4 Other material / equipment

Tab. 3.4: Other material used for experiments.

Material	Supplier
Biopore membranes	Millipore, Billerica, USA
Electro-optical modulators	Conoptics, Danbury, USA
Gatan Orius SC1000 CCD camera and software Gatan DigitalMicrograph	Gatan, Pleasanton, USA
Gold particles	Bio-Rad, München, Germany
Helios Gene Gun System	Bio-Rad, München, Germany
JEOL JEM-1230 transmission electron microscope	Jeol, Tokyo, Japan
Mai Tai Ti:Sapphire laser	Newport-Spectra Physics, Santa Clara, USA
Mcllwain tissue chopper	Mickle Laboratory Engineering, Surrey, United Kingdom
Millennia/Tsunami Ti:Sapphire laser	Newport-Spectra Physics, Santa Clara, USA

Material	Supplier
Millicell cell culture inserts (catalogue number PICMORG50)	Millipore, Billerica, USA
Nylon mesh	Klein & Wieler, Königswinter, Germany
Objective for two-photon microscope	Olympus, Tokyo, Japan
Parafilm	Pechiney Plastic Packaging, Des Moines, USA
Photomultipliers	Hamamatsu, Tokyo, Japan
Quiagen Maxi Prep Kit	Quiagen, Hilden, Germany
Toohey Picospritzer	Toohey Company, Fairfield, USA
Ultrastainer	Leica Microsystems, Wetzlar, Germany
Ultracut E microtome	Reichert-Jung, Buffalo, USA
Ultramicrotome EM UC6	Leica Microsystems, Wetzlar, Germany
Yanus IV laser scanner	Till Photonics, Gräfelfing, Germany
Zeiss Axiophot microscope for photo-oxidation of NIRB marks	Carl Zeiss Microscopy, Göttingen, Germany

3.2 Methods

3.2.1 Preparation of hippocampal slice cultures

Organotypic hippocampal slice cultures were prepared from P7-P8 Wistar rats and cultured according to the protocol of Stoppini et al. (Stoppini et al., 1991): Rats were killed by decapitation, skin and skull were removed and the hippocampi were resected in slice-preparation medium. Afterwards, the hippocampi were put on a McIlwain tissue chopper, cut into 400 μm thick transversal slices and immediately placed back into slice-preparation medium. Slices were then incubated for 30 minutes at 4°C and afterwards transferred onto Biopore membranes (pore size: 0.4 μm ; one slice per membrane). Slices on Biopore membranes were placed in Millicell cell culture inserts (pore size: 0.4 μm , diameter: 30 mm, height: 5 mm; 3 slices per insert) for incubation (35°C, 5 % CO₂) for 20 days. Half of the volume of slice culture medium was renewed every 3-4 days.

3.2.2 Biolistic transfection of hippocampal CA1 cells

CA1 pyramidal cells in cultured slices were biolistically transfected according to McAllister (McAllister, 2000) using the Helios Gene Gun System: In brief, gold particles coated with DNA (25 µg tdTomato in combination with 25 µg PSD-95-EGFP or 25 µg EGFP-Homer1c (for two-photon microscopy of spine and PSD size) or 12.5 µg EGFP alone (for two-photon microscopy of spine size followed by electron microscopy) as well as cartridges for biolistic transfection were prepared as follows: 12.5 mg of 1.6 µm gold were mixed with 100 µL spermidine (0.05 M in H₂O), vortexed and sonicated. DNA was added and, after vortexing, DNA was precipitated to the gold particles by adding 100 µL of 1 M CaCl₂ dropwise. The solution was incubated for 10 minutes while being mixed several times in between. The gold particles were then washed 3 times with absolutely dry 100% ethanol, followed by resuspension in a total of 3 mL PVP solution (0.05 mg/mL PVP in absolutely dry 100% ethanol). Afterwards, cartridges were prepared by filling 75 cm long tubing (dried beforehand with nitrogen for 30 minutes) with the gold suspension and incubation of the suspension for 5 minutes. Then, the solution was removed, followed by another 5 minutes of incubation while rotating and drying the tubing with nitrogen at a pressure 0.35 LPM. Last, the tubing was cut into 1.3 cm long cartridges which were stored at 4°C. To keep the vials dry from moisture, a desiccant pellet was added to the vials, and the vials were sealed with parafilm.

Hippocampal slices were transfected at 4 days *in vitro* (DIV 4; day of preparation = DIV 0) with DNA coated gold particles at a pressure of 180 PSI (Helium gas) and at a distance of approximately 1 cm. A nylon mesh with 100 µm pore size in front of the barrel liner was used to diffuse the gold particles and to reduce effective pressure at the location of tissue penetration. Transfected slices were then kept in culture until used for experiments between DIV 7-20.

3.2.3 The principle of two-photon fluorescence laser scanning microscopy (TPLSM)

The two-photon fluorescence microscope (TPLSM) was developed by Winfried Denk in 1990 (Denk et al., 1990; Svoboda et al., 2006). In TPLSM, two photons of low-energy instead of one high-energy photon excite a fluorescent protein (Figure 3.1 A).

Because of the non-linear nature of this process, the excitation is limited to a tiny diffraction-limited volume ($\approx 1 \mu\text{m}^3$) (Figure 3.1 B). This localization of excitation provides contrast and resolution comparable to confocal microscopy without requiring spatial filters like pinholes. For imaging in brain slices TPLSM has three advantages over one photon microscopy. The longer wavelength excitation light penetrates better into tissue. Effectively absent excitation outside the focus reduces photodamage. Without the requirement for spatial filters fluorescence photons are collected more efficiently, allowing the use of reduced excitation power, which in turn further reduces photodamage.

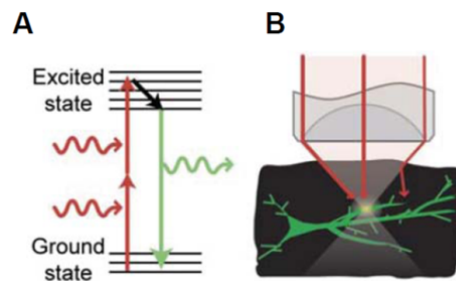


Figure 3.1: Principle of two-photon excitation microscopy.

(A) Simplified Jablonski diagram of the two-photon excitation process. Instead of one photon two photons of approximately the double wavelength are absorbed, leading to an excited electron state. After some of the energy is released radiationless by internal conversion, a single photon is emitted, with a longer wavelength compared to the one of the excitation photons.

(B) Localization of excitation in a scattering medium (black). The excitation beam (red) is focused to a diffraction-limited spot by an objective where it excites a green fluorophore in a dendritic branch, but not in a nearby branch. The paths of two ballistic photons and one scattered photon are shown (red lines). Scattered photons are too dilute to cause off-focus excitation. The intensity of the beam decreases with depth as an increasing number of excitation photons are scattered. Adapted from Svoboda et al., 2006.

3.2.4 The principle of glutamate uncaging

Glutamate uncaging serves as an efficient method to induce plasticity at single spines (Matsuzaki et al., 2004): the neurotransmitter glutamate is generated from the chemical compound MNI-caged-L-glutamate (4-methoxy-7-nitroindoliny-caged-L-glutamate) by photolysis using a 720 nm two photon excitation laser beam (Figure 3.2). After uncaging, glutamate can bind to AMPA and NMDA receptors. Matsuzaki et al. showed that glutamate uncaging induces a

rapid and selective enlargement of stimulated spines as well as an increase in postsynaptic responsiveness.

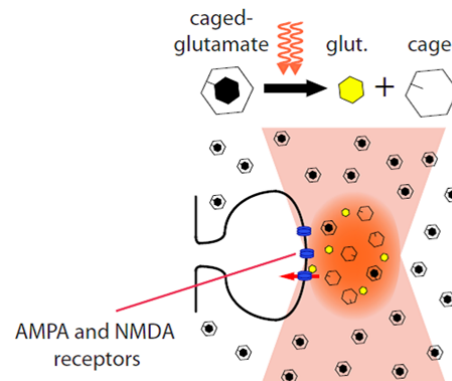


Figure 3.2: Principle of two-photon glutamate uncaging.

Top: Photolysis releases glutamate from its chemical cage MNI. Bottom: Glutamate is released locally within a very small defined volume close to a dendritic spine, leading to activation of AMPA and NMDA receptors.

Glutamate uncaging has several advantages over alternative plasticity induction methods such as electrophysiological stimulation or chemical LTP induction: first, nerve cell tissue does not need to be impaled by a pipette, avoiding any mechanical damage and saving time. Furthermore, by using two-photon excitation, glutamate uncaging is localized in a very small defined focal volume, which allows inducing plasticity specifically at single spines.

3.2.5 Combination of two-photon time-lapse imaging and glutamate uncaging

Imaging experiments were carried out at 35 °C in ACSF (artificial cerebrospinal fluid), saturated with carbogen. ACSF contained TTX, which was necessary to induce persistent spine growth, probably because TTX prevents competition between stimulated and neighbouring spines by blocking activity. To facilitate NMDA receptor activation, no Mg^{2+} was added to the bathing solution. Only mushroom-like spines, which are considered as mature postsynapses, were studied.

Two-photon laser-scanning microscopy was performed with a custom microscope (objective: 60X, 0.9 numerical aperture) (Figure 3.3). The light beams from two Ti:Sapphire lasers, one for imaging (Mai Tai, imaging intensity: 20 mW, measured in objective back aperture) the other (Millennia/Tsunami) for glutamate uncaging, were combined with a polarizing beam splitting cube and

scanned by the same scanner (Yanus IV laser scanner). The intensity of each beam was independently controlled with electro-optical modulators (350-80 LA) (Pockels cells). Photomultipliers recorded both epi- and transfluorescence. Image acquisition and uncaging were controlled by custom software written in Labview, version 8.6 (National Instruments, Austin, USA).

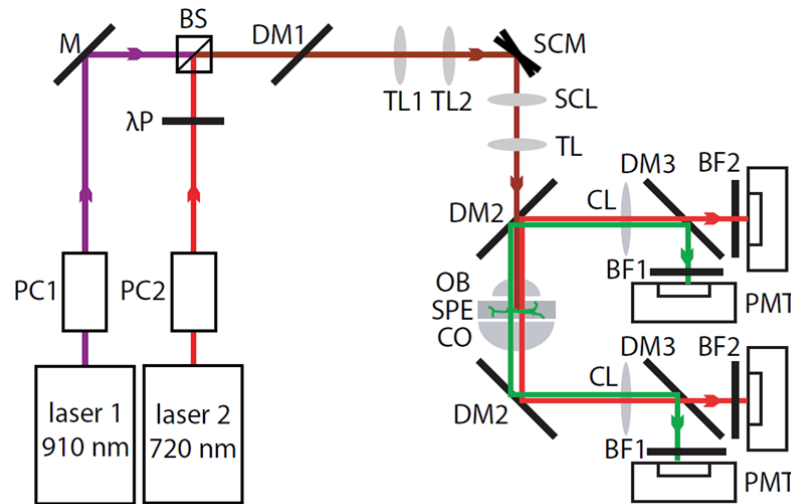


Figure 3.3: Schematic drawing of the optical setup used for imaging and glutamate uncaging.

BF: band pass filter, BS: beam splitting cube, CL: collector lens, CO: condenser, DM: dichroic mirror, M: mirror, OB: objective, PC: Pockels cell, PMT: photomultiplier tube, SC: scan mirrors, SCL: scan lens, SPE: specimen, TL: telescope lens, λP : λ half wave plate. Laser beam 1 and 2 are combined with a polarizing beam splitting cube and steered to the specimen. Epi- and transfluorescent emitted signals are detected by photomultiplier tubes in a 2-channel mode. Laser beam intensity is regulated by Pockels cells.

For uncaging, 3 μ L of MNI-caged-L-glutamate (stored at -20°C in aliquots of 15 μ L for a maximum of 3 months) were filled into a glass pipette (tip diameter ca. 10 μ m) and applied locally by puff application using a Toohey picospritzer. For this purpose, the pipette tip was positioned slightly above the surface of the slice close to the xy location of the spine to be stimulated.

Experimental timeline was as follows: first 7 images were taken at an interval of 2 minutes (baseline). MNI-caged-L-glutamate was applied from 1 minute before uncaging until the end of stimulation. Uncaging was performed close to the spine to be stimulated (30 pulses at 0.5 Hz, 4 ms pulse duration, 20-80 mW at the objective back aperture depending on depth in the slice). Only mushroom-like spines residing on apical dendritic branches (and not on the dendritic stem) were stimulated. Within 30 seconds after stimulation an image

was taken, followed by another image 60 seconds after stimulation. From then on images were taken every 5 minutes for 1 hour, and then - in case of experiments over 3 hours - every 10 minutes until the end of the experiment. In the text and in the figures, values 1 hour after stimulation represent averaged values for the time bin 45 to 75 minutes after stimulation, and values 3 hours after stimulation represent averaged values for the time bin 155 to 185 minutes after stimulation.

3.2.6 Forskolin application

The experiments with forskolin application were performed according to the experimental timeline described above, except for forskolin application during plasticity induction: Forskolin-ACSF was washed into the perfusion chamber rapidly within 2 minutes after the baseline recording, slices were then incubated in that solution for 5 minutes, followed by local MNI-caged-L-glutamate application for 1 minute and subsequent glutamate-uncaging. Two minutes after glutamate-uncaging, forskolin-ACSF was replaced again by forskolin-free ACSF within 2 minutes.

3.2.7 Near infrared branding (NIRB)

For electron microscopical analysis, time-lapse imaging after plasticity induction was performed as described above in section 3.2.5. After the acquisition of the last imaging time point, slices were immediately transferred into fixative. For control experiments, the last time point was after baseline recording, and for uncaging experiments 3 hours after stimulation. Slices were fixed at 4°C for 12 - 60 h and then processed for electron microscopy following standard procedures (according to Knott et al., 2009).

After fixation, the spines which previously were studied by two-photon microscopy, were located and marked by near infrared branding (NIRB) (Bishop et al., 2011) (Figure 3.4). Brandings were performed using the Mai Tai Ti:Sapphire laser tuned to 900 nm at a power of 200 mW (measured at back focal plane of objective). Several asymmetric rectangles were drawn around the structure of interest for unambiguous identification during photo-oxidation and electron microscopy (Figure 3.4).

For photo-oxidation of NIRB marks, slices were washed 4x in 100 mM Tris buffer for 10-20 min and transferred into diaminobenzidine solution (1.4 mg / mL

in 0.12 M Tris buffer). Photo-oxidation of NIRB marks was carried out by exciting the region at 510-560 nm for 35-40 min with a 40x objective (microscope: Zeiss Axiophot). Afterwards slices were washed again 4x in 100 mM Tris buffer for 10-20 min, followed by washing 4x in 100 mM sodium cacodylate buffer for 15 min.

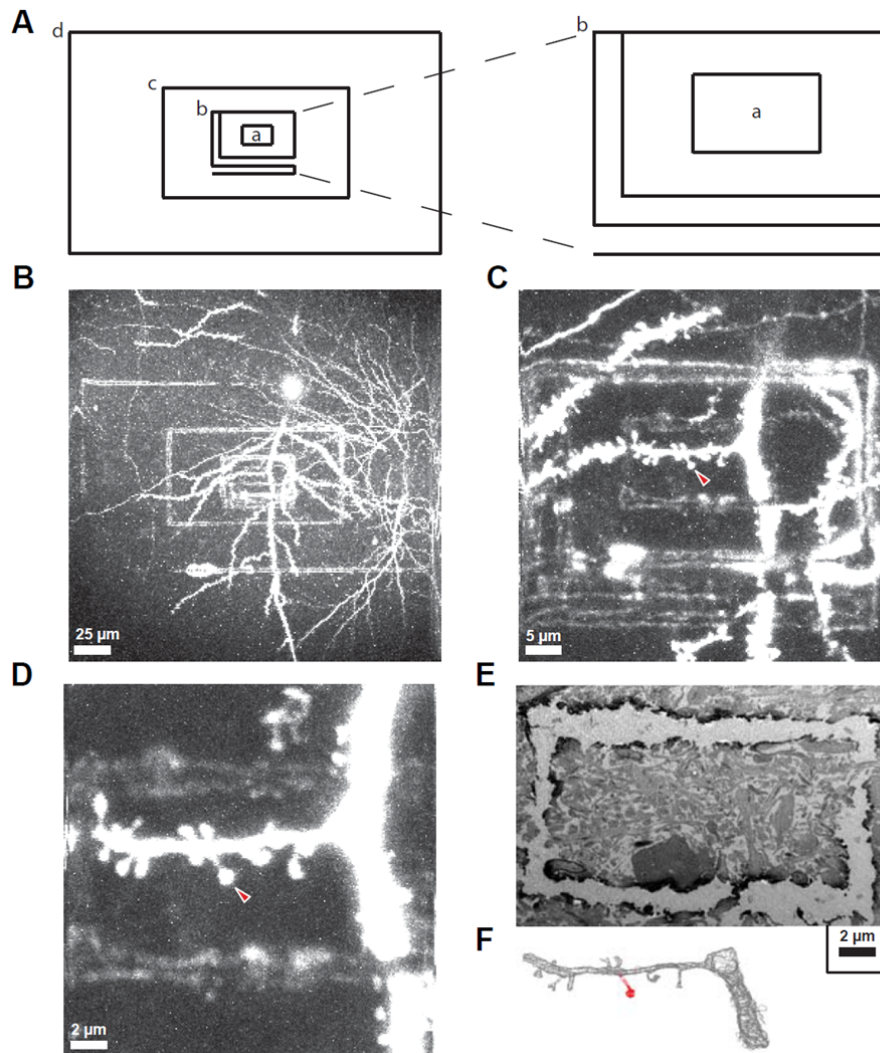


Figure 3.4: Scheme illustrating the pattern of the branding produced by NIRB.

(A) Schematic drawing of the NIRB pattern used for identification of the structure of interest. Dimensions: rectangle (a): ca. 21x12 μm , rectangle (b): ca. 50x29 μm , rectangle (c): ca. 125x73 μm , rectangle (d): ca. 250x145 μm . z-distances between rectangles: (a-b): 2 μm , (b-c): 5 μm , (c-d): 5 μm (with rectangle (d) being the most upper one).

(B-D) Fluorescence images of the NIRB pattern enclosing a neuron, its dendritic branch and its spines at different zooms. Arrowhead marks a stimulated spine.

(E) Image of an EM section showing the smallest NIRB rectangle (rectangle (a) in (A)).

(F) Reconstruction of the dendritic structure marked by NIRB. The stimulated spine is presented in red.

3.7.8 Electron microscopy

Osmication was done in 1% OSO_4 in 100 mM sodium cacodylate for 40 min. Afterwards slices were washed 3x in distilled water. Slices were then dehydrated successively in 50%, 70%, 2x 100% ethanol, and 100% propylene oxide for 10 min, respectively, followed by equilibration in 100% propylene oxide / resin for 24 hours. Afterwards, slices were transferred into 100% resin, equilibrated for 2 hours, and then embedded in fresh resin for 48 hours at 60°C. Embedded slices were first cut into 1 μm thick sections using a Reichert-Jung Ultracut E microtome until the NIRB marks of rectangle b (see Figure 3.4 A) were located. Then, ultrathin serial sections were cut (ca. 100-200 sections, dimensions 150 μm x 250 μm , 70 nm thickness) on an Ultramicrotome EM UC6. Samples were counterstained in a Leica Ultrastainer with 0.5% uranyl acetate and 3% lead citrate. Images were acquired on a JEOL JEM-1230 transmission electron microscope (80 kV) with a Gatan Orius SC1000 CCD camera (software: Gatan DigitalMicrograph).

3.2.9 Image analysis

Spine volume (tdTomato fluorescence) and amount of PSD protein (EGFP fluorescence) were determined as follows: image frames were median filtered in a 3x3 neighbourhood. Then, the maximum projection of the median filtered frames was calculated, and the signal within the region of interest (ROI) was again median filtered in a 5x5 neighbourhood. Afterwards, the dark current, determined as medium signal of a dark frame recorded before each stack, was subtracted. Remaining background noise was calculated from the median of the maximum projection, and subtracted. Last, the contribution of the cytosolic protein fraction to the spine PSD-95 / Homer1c signal was estimated by using the average value calculated from 3 different ROIs on the dendrite (assuming all protein in the dendrite is cytosolic) and subtracted.

In electron microscopy experiments spine fluorescence volumes were determined from EGFP fluorescence. The imaged dendritic segments were reconstructed from linearly aligned EM images at a magnification of 8000 using the software Reconstruct (version 1.1.0.0, <http://synapses.clm.utexas.edu/tools/index.stm>) (Fiala, 2005) to identify the stimulated or control spines of interest (Figure 3.4 F). For

measurements of spine volume, PSD area and bouton volume the identified synapses were imaged again at a magnification of 50 000 and reconstructed.

3.2.10 Data analysis

Data were analyzed with custom routines written in Matlab (version R2010a, The Mathworks, Natick, MA, USA). Data are reported as mean \pm standard error of the mean (SEM). In case data were normalized to spines on same dendritic segment, at least 4 spines were used for normalization. Statistical comparisons were performed with one-sample or two-sample one- or two-tailed Student's t-test for normally distributed data and with Wilcoxon signed rank test or Wilcoxon-Mann-Whitney test for not normally distributed data as indicated. Data were tested for normality using the 2-sided Shapiro-Wilk test for platykurtic samples and the Shapiro Francia test for leptokurtic samples (both combined in "swtest"):

<http://www.mathworks.com/matlabcentral/fileexchange/13964-shapiro-wilk-and-shapiro-francia-normality-tests/content/swtest.m>). The number of spines / number of cells in the individual experiments is sometimes abbreviated in the format n = x/y.

4. Results

4.1 Expression of PSD-95 and Homer1c as structural marker proteins of the PSD

To monitor simultaneously changes in spine volume and PSD size during plasticity, the cytosolic marker protein tdTomato, and one of the EGFP-tagged PSD scaffolding proteins, PSD-95 or Homer1c, as reporter for PSD size (see introduction), were expressed in CA1 pyramidal cells of cultured hippocampal slices. As shown in Figure 4.1, PSD-95-EGFP and EGFP-Homer1c were clearly localized to dendritic spines. This first section of the results part covers the suitability of PSD-95 and Homer1c as reporter proteins of PSD size, and the correlation of the amount of these proteins with spine volume under naïve conditions.

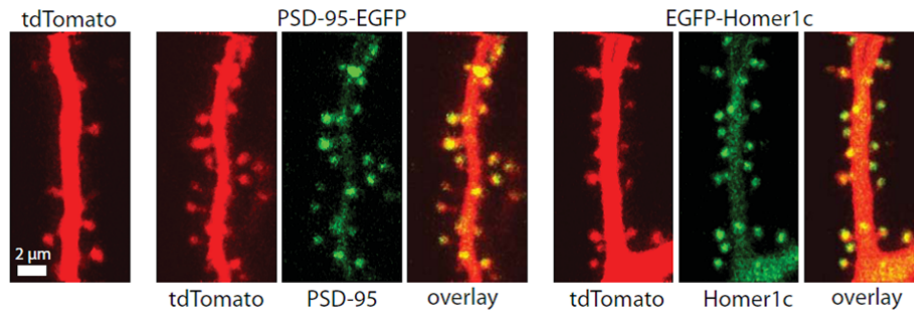


Figure 4.1: Labelling of spine and PSD proteins.

Two-photon images of dendritic segments from biolistically transfected pyramidal cells in hippocampal slice cultures, expressing tdTomato alone, tdTomato + PSD-95-EGFP and tdTomato + EGFP-Homer1c.

4.1.1 Overexpression of PSD-95 and Homer1c does not have a dramatic effect on spine volume and plasticity induction

Before starting my actual experiments, I first wanted to exclude the possibility that the overexpression of PSD-95 and Homer1c has any severe impact on spine volume or plasticity induction in my model system, which might question the validity of my experimental approach. Stein et al. for example observed that the overexpression of PSD-95 can occlude LTP (Stein et al., 2003), and Nikonenko demonstrated a dramatically increased spine volume of about 150% due to PSD-95 overexpression (Nikonenko et al., 2008). On the other hand

both PSD-95 and Homer1c were also used in other studies to explore synaptic plasticity or its underlying molecular mechanisms, without the observation of severe overexpression effects (Gray et al., 2006; Steiner et al., 2008; Petrini et al., 2009).

In my experiments the overexpression of PSD-95 was sufficiently low to cause only a small increase of about 25% in average spine size compared to neurons expressing tdTomato alone (tdTomato + PSD-95, volume = 23 ± 2 (a.u.), $n = 51$ spines / 13 cells; tdTomato alone, volume = 18 ± 1 (a.u.), $n = 51$ spines / 10 cells; $p = 0.014$, Wilcoxon rank sum test). Similarly, overexpression of Homer1c had no significant effect on spine size (tdTomato + Homer1c, volume = 16 ± 1 (a.u.), $n = 50$ spines / 9 cells; tdTomato alone, volume = 18 ± 1 (a.u.), $n = 51$ spines / 10 cells; $p = 0.122$, two-tailed t-test) (Figure 4.2 A).

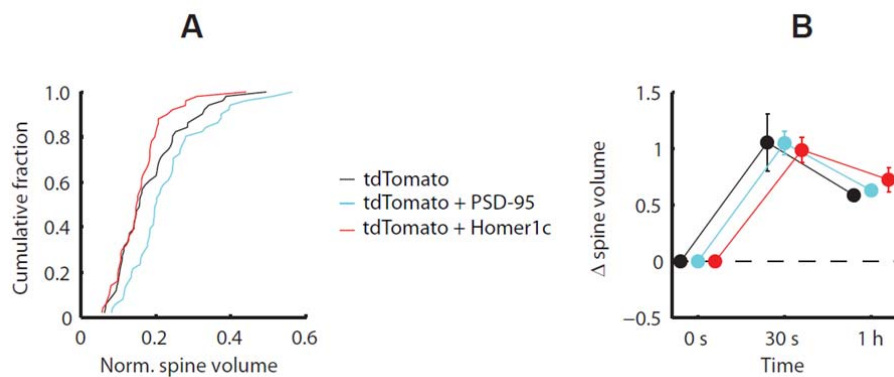


Figure 4.2: Overexpression of PSD-95-EGFP and EGFP-Homer1c does not have a dramatic effect on the volume of naïve spines and spine enlargement during structural plasticity.

(A) Spine volumes of cells expressing the proteins as shown in Figure 4.1 (tdTomato, $n = 51$ spines / 10 cells; PSD-95, $n = 51$ spines / 13 cells; Homer1c, $n = 50$ spines / 9 cells). Spine fluorescence data were normalized to fluorescence in a thick dendritic segment.

(B) Changes in spine volume 30 seconds and 1 hour after stimulation, normalized to pre-stimulation baseline (tdTomato, $n = 11$ spines / 8 cells; PSD-95, $n = 37$ spines / 37 cells; Homer1c, $n = 14$ spines / 14 cells).

Furthermore, neither overexpression of PSD-95 nor Homer1c demonstrated a significant impact on the spine growth rate immediately after stimulation and 1 hour later (tdTomato vs. PSD-95: Δ spine volume 30 s after stimulation: $105 \pm 25\%$ vs. $103 \pm 11\%$, $p = 0.540$, Wilcoxon rank sum test; Δ spine volume 1 h after stimulation: $59 \pm 5\%$ vs. $64 \pm 6\%$, $p = 0.902$, Wilcoxon rank sum test; tdTomato vs. Homer1c: Δ spine volume 30 s after stimulation: $105 \pm 25\%$ vs. $102 \pm 11\%$, $p = 0.524$, Wilcoxon rank sum test; Δ spine volume 1 h after

stimulation: $59 \pm 5\%$ vs. $78 \pm 13\%$, $p = 0.299$, two-tailed t-test; tdTomato, $n = 11$ spines / 8 cells; PSD-95, $n = 37$ spines / 37 cells; Homer1c, $n = 14$ spines / 14 cells) (Figure 4.2 B).

From these results I concluded that the overexpression of PSD-95 or Homer1c should not dramatically alter the physiology of my experimental system with respect to the explored questions.

4.1.2 Spine volume and PSD marker protein level correlate under naïve conditions

Next, I tested whether PSD-95 and Homer1c, which are abundant and important scaffolding proteins of the PSD, are suitable reporter proteins for the size of the PSD (Sheng et al., 2007). If this would be true PSD-95 and Homer1c levels should correlate similarly with the spine volume as it was shown for the PSD and spine volume in electron microscopy experiments (Harris et al., 1989; Schikorski et al., 1999; Arellano et al., 2007). Indeed, the level of both PSD-95 and Homer1c showed a significant correlation with spine volume (PSD-95, $R = 0.75$; $p < 0.001$, $n = 76$ spines / 17 cells; Homer1c, $R = 0.86$; $p < 0.001$, $n = 76$ spines / 15 cells) (Figure 4.3).

Together with the results from 4.1.1, this confirms that both GFP-tagged PSD-95 and Homer1c can serve as appropriate reporter proteins for PSD size.

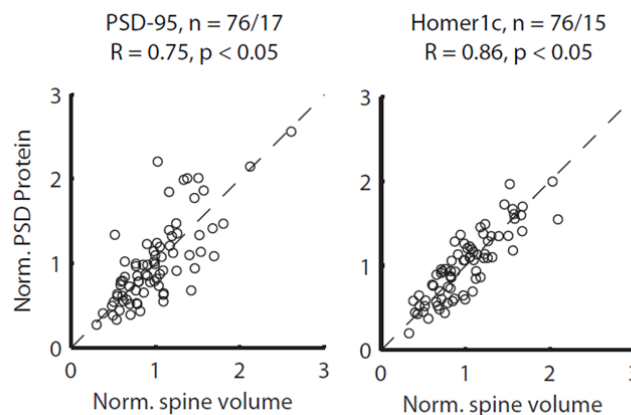


Figure 4.3: Correlation between spine volume and PSD size in naïve spines.

Correlation of PSD-95 (left) and Homer1c level (right) with spine volume; parameter of individual spines were normalized to mean of all spines from the same dendritic segment. R = correlation coefficient, p = significance of correlation.

4.2 Plasticity induction leads to increase in spine volume and PSD marker proteins

4.2.1 Spine volume and the amount of PSD scaffolding proteins increase within one hour after spine stimulation

After having demonstrated that PSD-95 and Homer1c are appropriate reporter proteins for the size of the PSD, I explored the structural plasticity of spines and their PSD. For this purpose, single spines of small to medium size were stimulated by focal two-photon glutamate uncaging, which has been shown to induce persistent spine enlargement and potentiation of AMPA-receptor-mediated currents reminiscent of long-term potentiation (Matsuzaki et al., 2004; Harvey et al., 2007).

To rule out any effect of two-photon illumination on spine volume and PSD marker proteins during uncaging, I executed two-photon uncaging protocols at single spines ($n = 3$ spines / 3 cells) without adding MNI-caged-L-glutamate. No effect was observed.

I then stimulated single spines by actual glutamate uncaging. Figures 4.4 A-D show example images and traces for changes in spine volume and PSD reporter signal after spine stimulation. The first example demonstrates enlargement of a stimulated spine, which is accompanied by a mild increase in PSD-95. In the second example a parallel increase of a stimulated spine and its Homer1c level is observed. In the illustrated neighbouring spines no increase occurred, neither in spine volume nor PSD signal.

For further analysis, only spines were included which displayed an average volume increase $> 20\%$ in the time bin of 1 hour (45-75 min) after stimulation. This value corresponds to the average standard deviation of spine volume fluctuations during the baseline prior to stimulation. Because signalling molecules diffuse from stimulated spines into the dendrite and can have effects on neighbouring spines (Harvey et al., 2007; Harvey et al., 2008), rather than using neighbouring unstimulated spines as controls I performed separate control experiments by imaging unperturbed spines.

In these control experiments no glutamate was added, and no two-photon stimulation protocol was executed. Surprisingly, in the control experiments I observed on average a significant decline of the PSD-95 signal over the time period of 1 hour ($-12 \pm 3\%$, $n = 36$ spines / 9 cells; $p = 6.612 \cdot 10^{-4}$, one sample t-test) (compare Zhang et al., 2011) (Figure 4.5 A). In contrast, the Homer1c signal

in control experiments remained stable over time ($4 \pm 6\%$, $n = 33$ spines / 10 cells; $p = 0.999$, one sample t-test) (Figure 4.5 C). Therefore, in the following the data for the PSD-95 level in stimulated spines were corrected for the PSD-95 decline in control experiments.

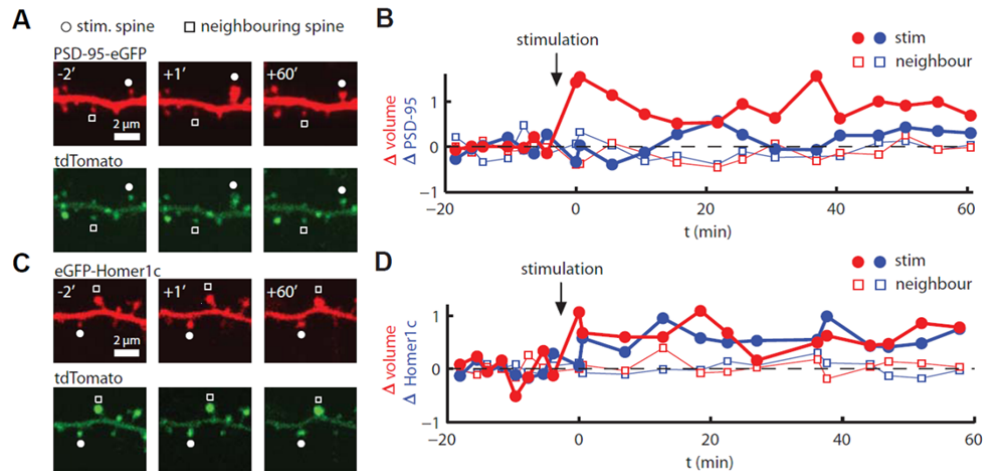


Figure 4.4: Examples for a typical PSD-95 and Homer1c experiment.

(A) Images of dendritic segment co-expressing tdTomato and PSD-95-EGFP before and after plasticity induction by glutamate uncaging.

(B) Time course of spine volume (red) and PSD-95 level (blue) in stimulated spine (filled circles) and unstimulated neighbouring spine (open squares). Data are normalized to pre-stimulation baseline.

(C,D) Same as in (A,B) but for Homer1c.

In stimulated spines, the PSD-95 signal increased on average slowly, 1 hour after stimulation it was increased by $19 \pm 4\%$ ($n = 37$ spines / 37 cells) relative to control ($p = 8.447 \cdot 10^{-4}$, Wilcoxon rank sum test) (Figure 4.5 A). Compared to PSD-95, Homer1c increased rapidly within 20 minutes, and 1 hour after stimulation it was increased by $44 \pm 8\%$ ($n = 13$ spines / 13 cells; $p = 5.396 \cdot 10^{-4}$, two-tailed t-test) (Figure 4.5 C).

Consequently, both for PSD-95 and Homer1c, the protein increase was less than the increase in spine volume (PSD-95, $19 \pm 4\%$ versus $63 \pm 6\%$, $n = 37$ spines / 37 cells; $p = 2.748 \cdot 10^{-8}$, Wilcoxon rank sum test; Homer1c, $44 \pm 8\%$ versus $73 \pm 11\%$, $n = 13$ spines / 13 cells; $p = 0.047$, two-tailed t-test).

Furthermore, the PSD-95 signal increase was by a factor of 2 smaller than the increase in Homer1c signal ($p = 0.007$, Wilcoxon rank sum test), although the spine size increase was similar in both cases ($p = 0.342$, Wilcoxon rank sum test). This difference was not because in general the PSD-95 signal increase was less in

stimulated spines, but because a smaller fraction of spines displayed a PSD-95 increase comparable to their volume enlargement (Figure 4.5 B and D, data for stimulated spines are corrected for PSD-95 level decline in control experiments).

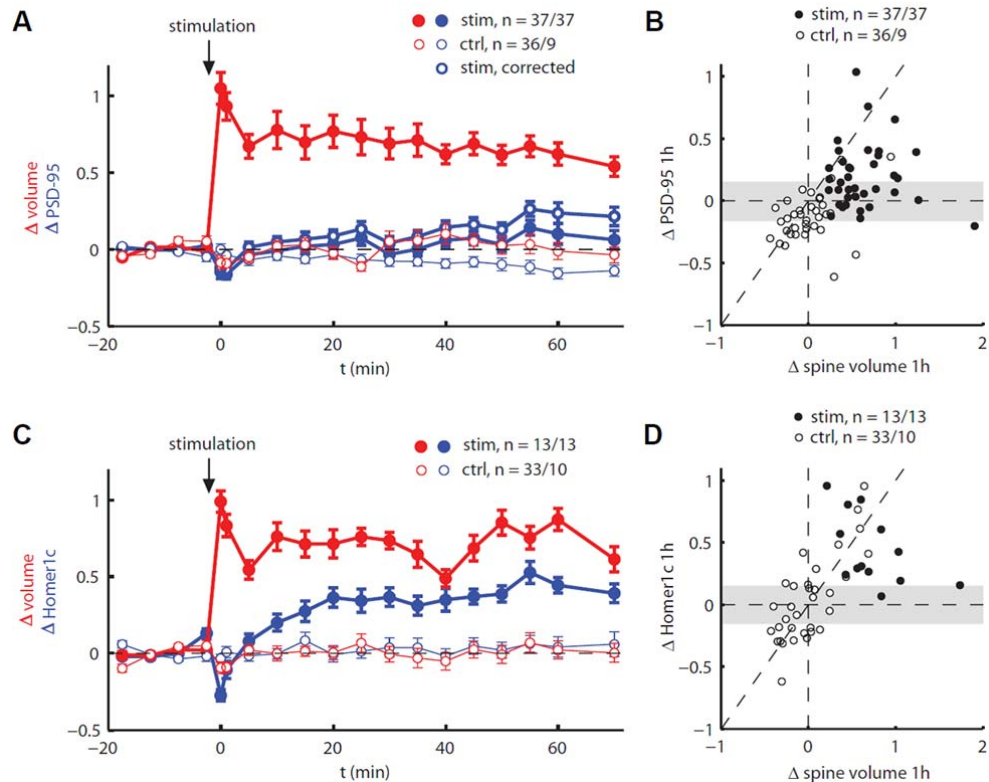


Figure 4.5: Glutamate uncaging induced increase in spine volume and in the amount of PSD scaffolding proteins over 1 hour.

(A) Mean change in spine volume (red) and PSD-95 (blue) of stimulated spines (heavy traces) compared to control (thin traces). Heavy trace with open circles represents increase in PSD-95 corrected for control. Error bars: SEM.

(B) Correlation between change of PSD-95 (corrected for control) and spine volume 1 hour after stimulation for stimulated spines (filled circles) and control spines (open circles); gray rectangle = mean standard deviation of PSD-95 baseline fluctuation.

(C) Same as in (A), but for Homer1c (without correction for control).

(D) Same as in (B), but for Homer1c (without correction for control).

Previously it has been reported that after induction of morphological spine plasticity PSD-95 transiently decreases and then remains unchanged at the initial level when exploring the first 30 min after stimulation (Steiner et al., 2008). Despite experimental differences between this report and my analysis, in particular Steiner et al. performed their recordings at room temperature, while I used physiological temperature (35 °C), together these observations suggest that

the expected reestablishment of the correlation between spine and PSD size requires more time.

4.2.2 Over a period of 3 hours spine volume and PSD size move towards a new balance at a larger overall size

To explore if the reestablishment of the correlation in spine and PSD size after plasticity induction occurs after an extended time, and furthermore to monitor the stability of structural changes, I performed additional experiments with 3 hour imaging periods after plasticity induction.

Over the 3 hour period the average PSD-95 level indeed continued to increase and reached $27 \pm 8\%$ ($n = 17$ spines / 17 cells) compared to $13 \pm 4\%$ after one hour in these experiments ($n = 17$ spines / 17 cells; $p = 0.082$, one-tailed t-test) (Figure 4.6 A). In contrast, the average Homer1c level did not increase further and remained essentially unchanged between 1 hour ($44 \pm 8\%$, $n = 13$ spines / 13 cells) and 3 hours ($38 \pm 12\%$, $n = 13$ spines / 13 cells; $p = 0.695$, two-tailed t-test) after stimulation (Figure 4.6 C).

Furthermore, the spine volume did not continue to increase from 1 to 3 hours after stimulation, but rather displayed a small drop both in PSD-95 (from $62 \pm 6\%$ to $49 \pm 8\%$, $n = 17$ spines / 17 cells; $p = 0.232$, two-tailed t-test) (Figure 4.6 A) and Homer1c experiments (from $73 \pm 11\%$ to $54 \pm 13\%$, $n = 13$ spines / 13 cells; $p = 0.289$, two-tailed t-test) (Figure 4.6 C).

Similar to 1 hour after stimulation, also 3 hours after plasticity induction the PSD-95 level were increased only in a subpopulation of stably growing spines (Figure 4.6 B). In contrast, for Homer1c experiments only in one stably growing spine the protein was not increased (Figure 4.6 D).

In addition, both in PSD-95 and Homer1c experiments, some spines did not stably increase over 3 hours. In most of these cases also PSD-95 and Homer1c ultimately were not increased (Figure 4.6 B and D).

In summary, with PSD-95 on average further increasing, Homer1c remaining unchanged and spine volume dropping over 3 hours compared to 1 hour after stimulation, PSD and spine move closer to be balanced at a larger overall size (PSD-95 $26 \pm 8\%$ versus volume $49 \pm 8\%$; $p = 0.065$, two-tailed t-test, Homer1c $38 \pm 12\%$ versus volume $54 \pm 13\%$; $p = 0.392$, two-tailed t-test).

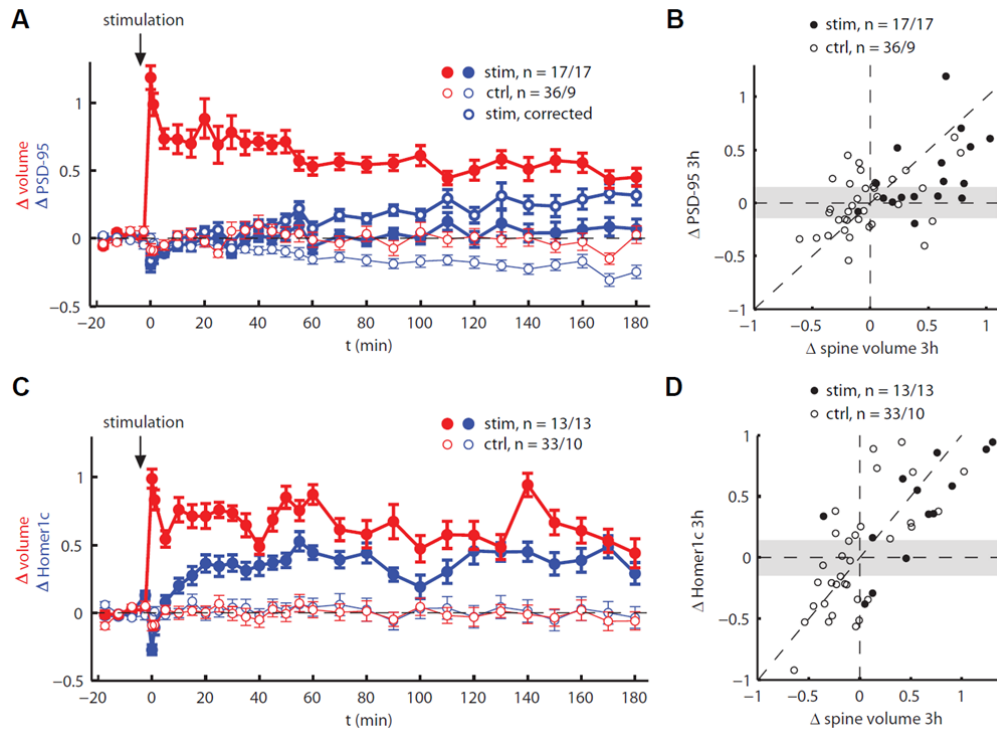


Figure 4.6: Glutamate uncaging induced increase in spine volume and in the amount of PSD scaffolding proteins over 3 hours.

(A) Mean change in spine volume (red) and PSD-95 (blue) of stimulated spines (heavy traces) compared to control (thin traces). Heavy trace with open circles represents increase in PSD-95 corrected for control. Error bars: SEM.

(B) Correlation between change of PSD-95 (corrected for control) and spine volume 3 hours after stimulation for stimulated spines (filled circles) and control spines (open circles); gray rectangle = mean standard deviation of PSD-95 baseline fluctuation.

(C) Same as in (A), but for Homer1c.

(D) Same as in (B), but for Homer1c.

4.2.3 The correlation between spine volume and PSD-95 / Homer1c level is maintained

The results from section 4.2.2 suggest that during structural plasticity both spine and PSD size increase towards a new balance. Now, I was interested how the correlation between spine volume and PSD size for individual stimulated spines develops after stimulation and whether it is maintained 3 hours after stimulation. Figure 4.7 shows that for both PSD-95 and Homer1c the correlation is transiently disrupted, but is reestablished after 3 hours either by concomitant increase of both spine volume and PSD-95, or by reversion of the spine volume enlargement.

Next I explored how the increase in synaptic structures compares to the correlation between spine and PSD size obtained in naïve spines (compare Figure 4.3). Figure 4.8 A and B show the PSD versus spine size relationships of stimulated spines at three time points, prior to stimulation and at 1 and 3 hours after stimulation, plotted on top of the PSD versus spine size relationship in naïve control spines. Stimulated spines (red points in Figure 4.8 A and B) display prior to stimulation a similar correlation in spine and PSD size as naïve control spines both in PSD-95 (ratio PSD-95 level / spine volume, stimulated spines: 1.11 ± 0.10 , $n = 10$ spines / 10 cells; control spines: 1.02 ± 0.04 , $n = 76$ spines / 17 cells; $p = 0.278$, Wilcoxon rank sum test) and Homer1c experiments (ratio Homer1c level / spine volume, stimulated spines: 1.02 ± 0.06 , $n = 10$ spines / 10 cells; control spines: 1.01 ± 0.03 , $n = 76$ spines / 15 cells; $p = 0.982$, two-tailed t-test) (Figure 4.8 C).

After stimulation, in PSD-95 experiments, at first the PSD-95 signal did not closely follow the increase in spine size, so that the 1 hour data points (red squares) in the PSD versus spine size diagram (Figure 4.8 A) shift to the right of the unity line and the ratio of PSD-95 level over spine volume significantly drops (1 h, 0.78 ± 0.03 ; baseline (= 0 h), 1.11 ± 0.10 , $n = 10$ spines / 10 cells; $p = 0.005$, two-tailed t-test) (Figure 4.8 C). With passing time, however, the size of both PSD-95 signal and spine size are readjusted such that 3 hours after stimulation the data points (red star symbols in Figure 4.8 A) scatter again around the unity line and the original correlation is reestablished at the population level (ratio PSD-95 level / spine volume, 3 h: 1.03 ± 0.09 , 0 h: 1.11 ± 0.10 , $n = 10$ spines / 10 cells; $p = 0.575$, two-tailed t-test) (Figure 4.8 C).

Overall, the Homer1c experiments showed essentially the same result as PSD-95 experiments, however, with a less pronounced and therefore insignificant transient drop in correlation (ratio Homer1c level / volume, 1 h: 0.87 ± 0.12 , $n = 10$ spines / 10 cells, 0 h: 1.02 ± 0.06 ; $p = 0.249$, two-tailed t-test; 3 h: 0.92 ± 0.08 , $n = 10$ spines / 10 cells, 0 h as above; $p = 0.366$, two-tailed t-test) (Figure 4.8 B and C).

Although the balance of spine size and PSD-95 signal was transiently disrupted after stimulation, the ratios of PSD signal over spine size of stimulated spines did essentially not decrease below the range of ratios in the naïve distribution, with two exceptions in the Homer1c experiments (Figure 4.8 A and B).

In conclusion, I found that 3 hours after spine stimulation the correlation between PSD size and spine volume in stimulated spines compares well with the correlation in naïve spines.

A

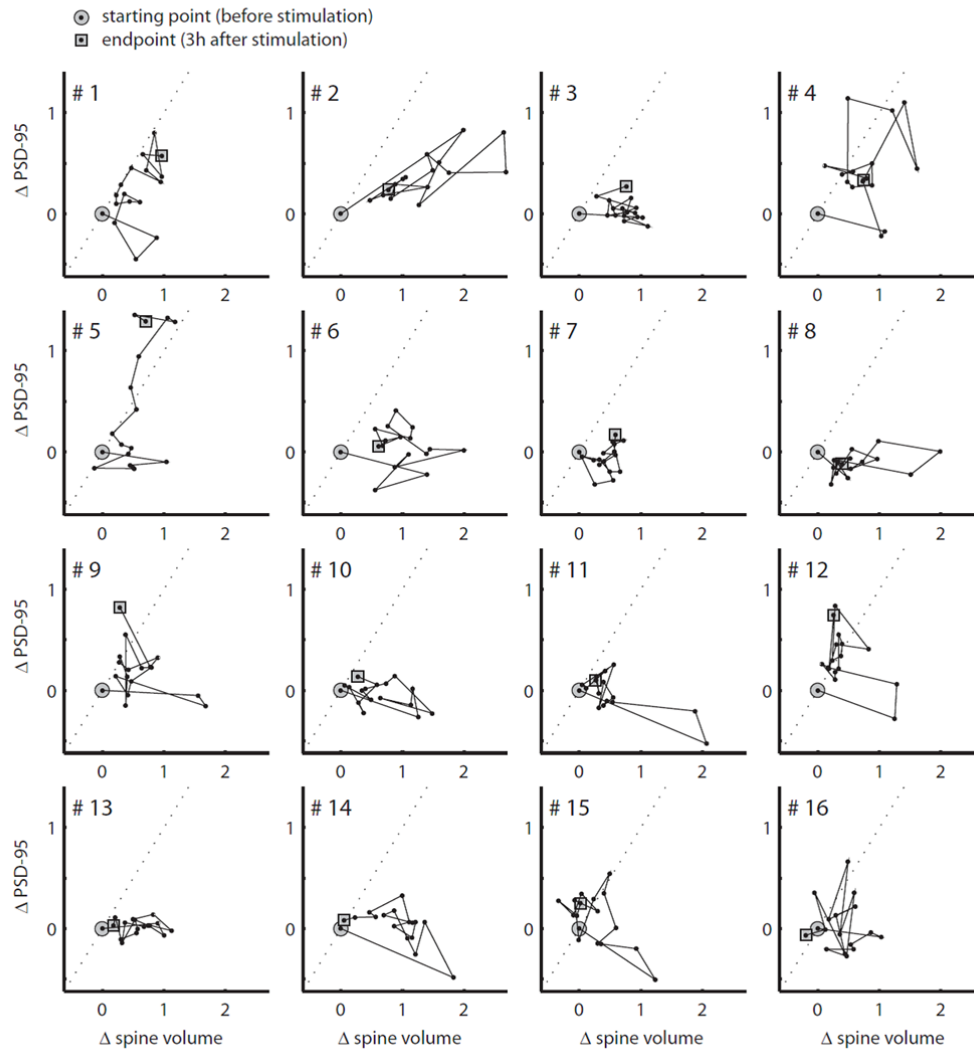


Figure 4.7: Figure continues on following page.

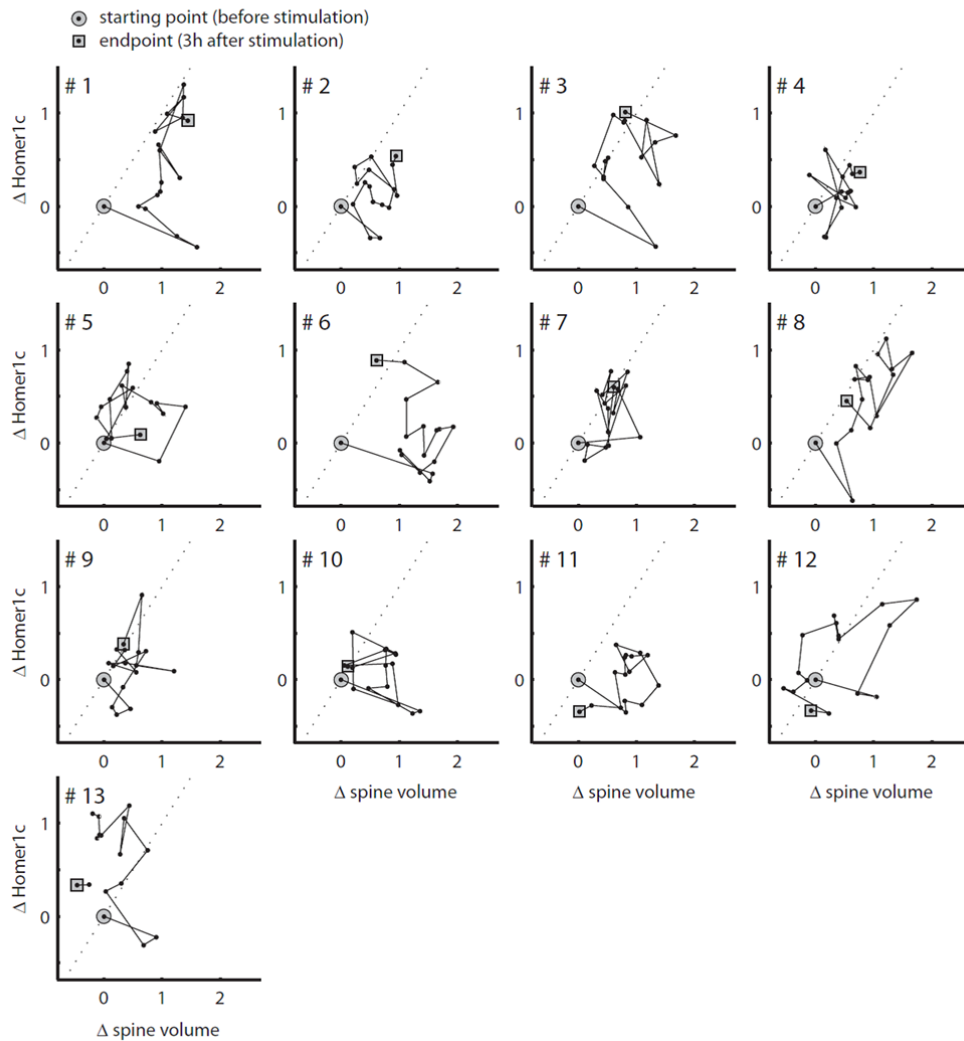
B

Figure 4.7: Time course of the PSD-volume relationship after plasticity induction.

(A) The relative change of PSD-95 signal is plotted versus the relative volume change over time for individual spines after stimulation. The circle marks the starting point before stimulation, the square the endpoint 3 hours after stimulation. The time between dots corresponds to 10 minutes for the first hour and 15 minutes for the second to third hour after stimulation, except for the initial four dots: The second dot is right after stimulation, the third 1 minute, and the fourth additional 5 minutes later. Spines were sorted according to the magnitude of their final volume change in descending order. In most cases the PSD-volume relationship displays after stimulation a marked rightward shift along the volume axis away from the unity line (dotted line) and then returns close to the unity line either by balancing volume and PSD-95 changes or by a reversion of the initial volume increase.

(B) Same as in (A) but for Homer1c.

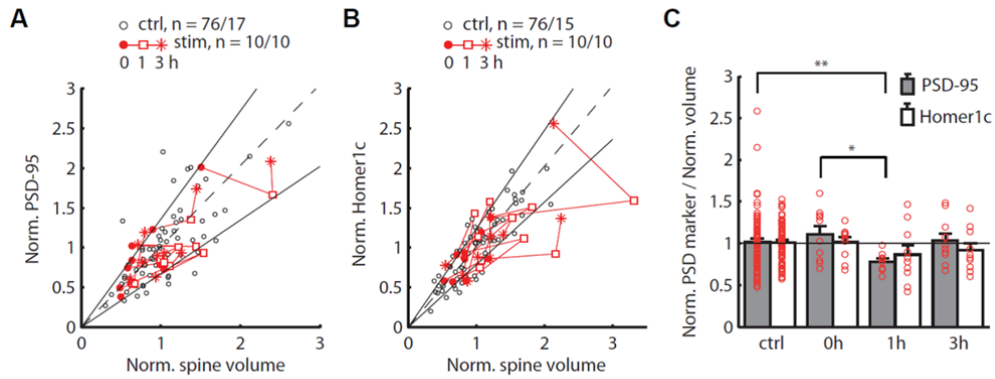


Figure 4.8: The volume-PSD correlation is maintained.

(A) Plot of PSD-95 level vs. spine volume before as well as 1 hour and 3 hours after stimulation on top of the naïve correlation of control spines (compare Fig. 4.3). Data were normalized to mean of all spines on dendritic segment. Dashed line: slope = mean of control data. Solid lines: slope = mean of control data \pm one standard deviation.

(B) Same as in (A) but for Homer1c data.

(C) Ratios of PSD marker level over spine volume for data in A,B. Circles: Individual spine data. Bars: mean value of ratios (PSD-95, control, n = 76 spines / 17 cells, stimulated 0h,1h,3h, n = 10 spines / 10 cells; Homer1c, control, n = 76 spines / 15 cells, stimulated 0h,1h,3h, n = 10 spines / 10 cells; error bars, SEM). Stars indicate significance: * = $p < 0.05$ (two-tailed t-test), ** = $p < 0.01$ (Wilcoxon rank sum test).

4.3 Stabilization of structural changes

4.3.1 Stabilization of structural changes goes in hand with the maintenance of the correlation between spine and PSD size

The results from 4.2.3 suggest that there is a connection between the stabilization of structural changes and the balancing of spine enlargement by a concomitant increase in PSD size, i.e. spines either stabilize at the increased volume along with an increase of the PSD, or their volume decays back to its original size without a significant increase of the PSD.

In the figures showing the spine volume increase at 3 hours versus 1 hour after stimulation (Figure 4.9 A and C), data on or above the unity line indicate that spine enlargement was unchanged or even increased, and data points below the unity line display that the spine enlargement decayed.

The majority of spines with unchanged or increased enlargement showed a strong increase in PSD protein (above the population mean; PSD-95: 27%, Homer1c: 38%; marked by filled circles), those with decaying enlargement a weak PSD protein increase (below mean increase; marked by open circles).

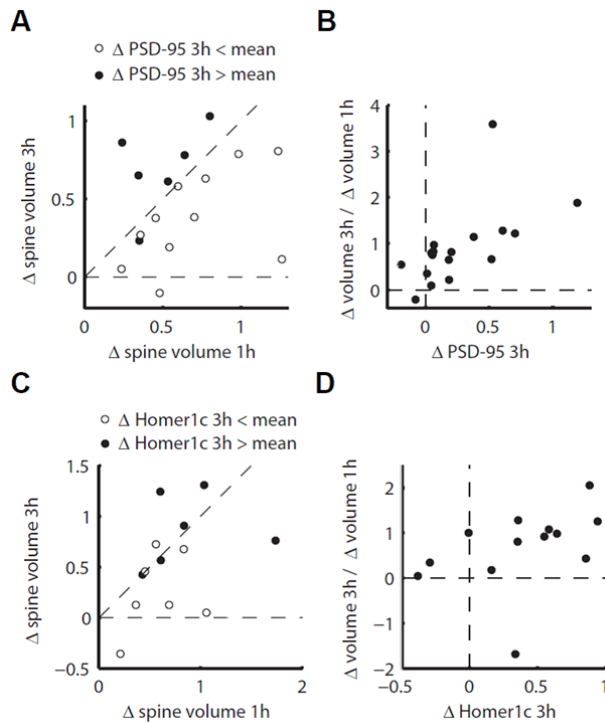


Figure 4.9: Stability of structural changes and the relationship to PSD size.

(A) Relationship between volume change at 1 and 3 hours after stimulation. In most cases where the gain in spine volume at 1 hour after stimulation is maintained or enhanced after 3 hours (data on and above the unity line) the PSD-95 level increase was greater than the population mean after 3 hours (filled circles, PSD-level increase > 27 %) and vice versa (open circles, PSD-level increase < 27 %).

(B) Ratio of volume gain after 3 hours over 1 hour versus PSD-95 level increase.

(C) As in (A) but for Homer1c data (strong increase > 38%; weak increase < 38%).

(D) As in (B) but for Homer1c.

Furthermore, the ratio of spine enlargement at 3 hours over 1 hour and the increase in PSD size at 3 hours after stimulation are roughly correlated (PSD-95, $R = 0.60$; $p = 0.010$, $n = 17$ spines / 17 cells; Homer1c, $R = 0.42$; $p = 0.157$, $n = 13$ spines / 13 cells) (Figure 4.9 B and D).

In summary, these results indeed support the idea that structural changes during plasticity are only stabilized if both spine volume and PSD increase together.

4.3.2 Detailed analysis of the time course of changes in PSD size and spine volume for spines with and without volume stabilization

Next, I explored the time point where the decision, whether or not the spine enlargement will be stabilized, becomes apparent. For this analysis I sorted my data into two groups, depending on whether the spine volume increase 3 hours after stimulation was strong and stabilized (enlargement > 40 %, i.e. twice the criterion for significant growth of 20 %) or weak and non-stabilized (enlargement < 20 %) (Figure 4.10). Spines which showed a stabilized but only small increase in volume (> 20 %, but < 40 %) were omitted, because the analysis

of the time courses required that both spine volume and PSD marker either demonstrated a robust increase or they did not.

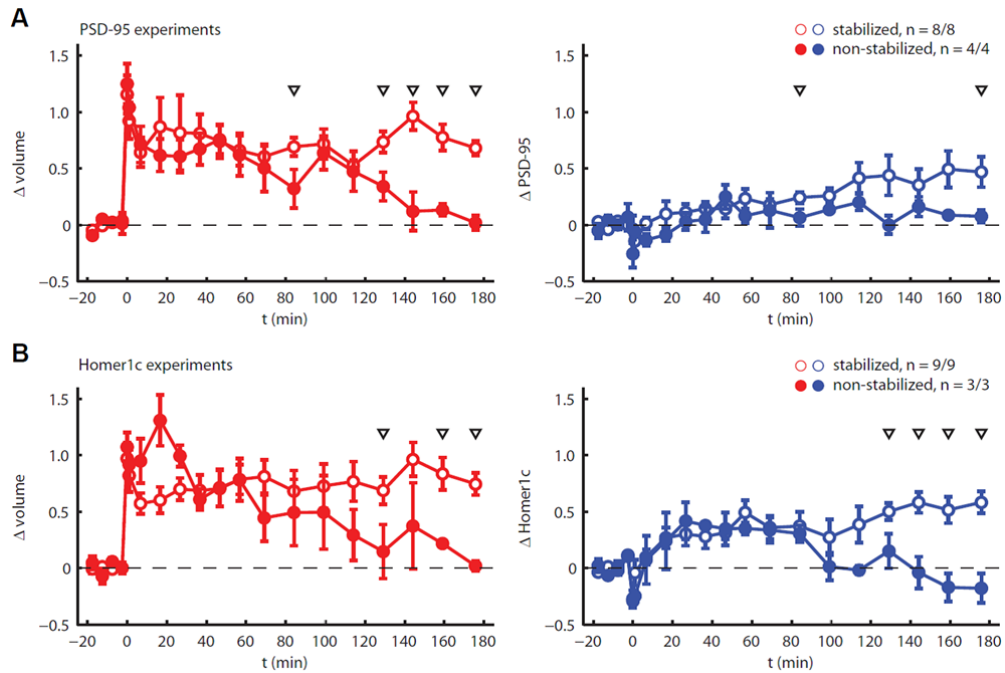


Figure 4.10: Time course of PSD size and spine volume changes for spines with and without stabilized enlargement.

(A) Left: Volume changes of spines with strong stabilized enlargement (open circles, final volume increase $> 40\%$, i.e. twice the criterion for enlargement) and non-stabilized enlargement (filled circles, final volume increase $< 20\%$). 4 spines of the PSD-95 data set displayed a stabilized but only small enlargement ($< 40\%$) and were therefore excluded from this analysis. Right: Changes in PSD-95 level for spines with strong stabilized and non-stabilized enlargement. Arrow heads mark time points with a significant difference between stabilized and non-stabilized spines ($p < 0.05$, one-tailed t-test).

(B) Same as in (A) but for Homer1c experiments. In the Homer1c data set in all cases of stabilized enlargement the increase was strong, i.e. $> 40\%$.

The two groups in both PSD-95 and Homer1c experiments displayed a similar spine volume increase immediately after stimulation. The PSD-95 signal dropped transiently in the two groups of spines (compare Steiner et al., 2008), and then increased slowly. At the time bin of 85 minutes, I found a first significant difference ($p_{\text{first}} = 0.047$, one-tailed t-test), with a higher PSD-95 signal in stabilized spines ($n = 8$ spines / 8 cells) compared to non-stabilized spines ($n = 4$ spines / 4 cells).

After that time point the PSD-95 signal continued to increase only in stabilized spines, whereas in non-stabilized spines it remained effectively unchanged. Interestingly, the time of divergence in PSD-95 signal and spine volume ($p_{\text{first}} = 0.036$ at 85 min, one-tailed t-test) occurred at the same time for both the stabilized and non-stabilized group (Figure 4.10 A).

In contrast to the PSD-95 signal, the Homer1c signal increased in a fast manner within 20 minutes after stimulation, and then remained effectively unchanged at an elevated level for a period of about 80 minutes both in stabilized and non-stabilized spines (Figure 4.10 B).

After that time the Homer1c signals started to diverge: In stabilized spines ($n = 9$ spines / 9 cells) the signal continued to increase slightly, whereas it decayed in non-stabilized spines ($n = 3$ spines / 3 cells). This difference became significant for the first time 130 minutes after stimulation ($p_{\text{first}} = 0.038$, one tailed t-test).

Also for the Homer1c data the divergence in the spine volume occurs roughly at the same time as the divergence in Homer1c signal, again becoming first significant at 130 minutes after stimulation ($p_{\text{first}} = 0.040$, one-tailed t-test) (Figure 4.10 B). Although this time point of the first significant difference is later than in PSD-95 experiments, overall the volume time course is very similar in PSD-95 and Homer1c experiments (compare Figure 4.10 A and B).

In summary, this suggests the following sequence of events: Stimulation directly leads to spine enlargement as shown before (e.g. Matsuzaki et al., 2004; Harvey et al., 2007). This is closely accompanied by an increase in Homer1c level, and only later by an increase in PSD-95 level in stabilized spines. In non-stabilized spines the absence of this last step appears to mark the onset of the decay of the volume enlargement, which is finally followed by the reversion of the initial Homer1c increase.

4.4 Forskolin application to promote L-LTP and PSD-95 increase

Next, I was interested in whether the pharmacological promotion of the stabilization of structural changes might accelerate the increase in PSD-95 during plasticity:

Activation of the PKA pathway by forskolin was shown to promote L-LTP induction (Govindarajan et al., 2011). At the level of spines, Govindarajan et al. reported that the application of forskolin during the time of glutamate uncaging

leads to an enlarged increase in spine volume. Furthermore, it supports the stabilization of induced spine volume changes (Govindarajan et al., 2011). Because a stabilization of spine volume increase should be associated with an increase in the PSD, the presence of forskolin during the time of spine stimulation might promote and maybe accelerate an increase in PSD-95 level. To elaborate on this possibility, I again performed time-lapse imaging of changes in spine volume and PSD-95 level. However, this time forskolin was applied during the time of plasticity induction (5 minutes before glutamate uncaging until 2 minutes after).

Rather surprisingly, I found that forskolin does not have a significant effect neither on spine volume growth nor on the increase in PSD-95 level (Figure 4.11, compare with Figure 4.6 A): The average volume increase was not altered, PSD-95 did not significantly increase faster or stronger, and the ratio of stabilized to non-stabilized spines was similar to experiments without forskolin (5:2 vs. 8:4, respectively). Interestingly, however, in forskolin control experiments PSD-95 level did not decrease compared to experiments without forskolin. This would speak for a role of forskolin in regulating global plasticity-related modifications rather than having a spine specific effect.

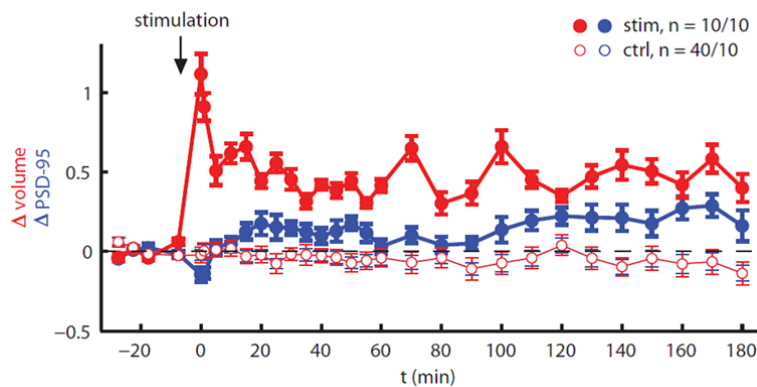


Figure 4.11: Forskolin does not have an effect on spine growth stabilization or on the increase in PSD-95 level after spine stimulation by glutamate uncaging.

Mean change in spine volume (red) and PSD-95 (blue) of stimulated spines (heavy traces) over time compared to control (thin traces). In control experiments forskolin was applied, but no uncaging was performed. Error bars: SEM.

Because in my experiments activity was blocked by TTX (in contrast to Govindarajan et al.), the global effect of forskolin might be disabled, and therefore also at the level of single spines no promoting effect on the stabilization of plasticity-related changes might be observed.

However, also the overexpression of PSD-95, although rather low in my experiments, might lead to the levelling of forskolin effects, due to a global increase of PSD-95 in spines.

4.5 Electron microscopy of synaptic structures after plasticity induction in spines

4.5.1 Electron microscopy experiments

So far I studied changes in important scaffolding proteins of the PSD, namely PSD-95 and Homer1c, as reporters for changes in PSD size. However, despite the structural and functional relevance of these two proteins within the PSD, they do not represent the PSD as a whole. In fact, the PSD consists of a multitude of different proteins (Kim et al., 2004). Therefore it was interesting to study changes of the PSD as an entity. In addition, I wanted to gain information on presynaptic changes during plasticity, i.e. volume changes of boutons associated with stimulated spines.

Therefore, in a final set of experiments, I analyzed stimulated spines with electron microscopy (EM) to confirm my results on structural plasticity of spine and PSD by ultrastructural reconstruction. In addition, I analyzed the size of the presynaptic boutons which contacted the stimulated spines. The structure of the active zone was hardly visible in my electron micrographs, and therefore it could not be analyzed. This difficulty was already described in previous electron microscopy studies (Schikorski et al., 1997) which solved the problem by applying a rather large error to the size of the measured active zones. Because of the expected magnitude of the error in my experiments I considered such a procedure as inappropriate.

The experimental procedure for my EM experiments was as follows: as for the PSD-95 experiments described above I imaged stimulated spines for 3 hours after stimulation. For control experiments I recorded 7 images separated by a time interval of 2 minutes. After imaging I fixed the slices and marked the imaged spines by near-infrared branding (NIRB) (Bishop et al., 2011) for electron microscopy. After EM, I determined spine and PSD size, and in addition bouton volume from ultrastructural reconstructions (Figure 4.12).

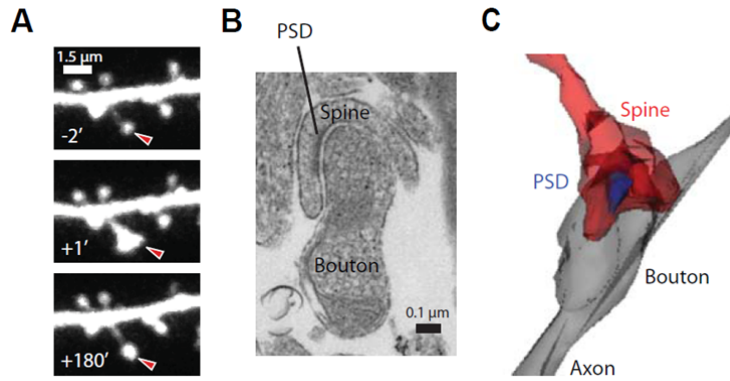


Figure 4.12: Electron microscopy of stimulated spines.

- (A) Spine in two-photon images before and after stimulation.
- (B) Spine from (A) on an EM section.
- (C) Spine from (A,B) reconstructed.

As proof of principle I compared EM spine volume and spine fluorescence in the two-photon microscope: EM spine volume and spine fluorescence correlated well (all imaged and reconstructed spines pooled together: $R = 0.67$, $p = 0.001$) (Figure 4.13). From this I concluded that changes in spine volume, which I measured via changes in spine fluorescence during imaging, should be reflected in the spine volume determined by electron microscopy.

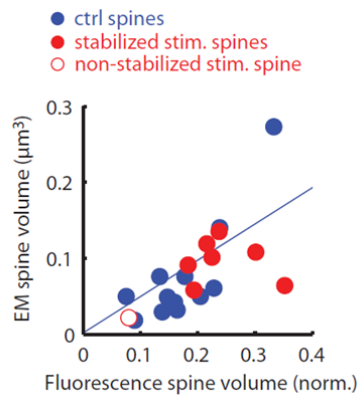


Figure 4.13: Relationship between EM spine volume and spine fluorescence in 2-photon microscopy.

EM spine volume over fluorescence spine volume for stimulated spines with persistent enlargement (red, filled circles), for a stimulated spine without persistent enlargement (red, open circle) and for control spines (blue, filled circles). Spine fluorescence was normalized to the fluorescence in a thick dendritic segment. Blue line: linear fit to control data.

The reconstruction of boutons showed that some of the analyzed spines (stimulated, 3 out of 7; control, 3 out of 12) had their synapse with multi-synapse boutons (MSBs) (Shepherd et al., 1998) (Figure 4.14 A), i.e. boutons which form synapses with more than one spine. Compared to spines contacting single-synapse boutons (SSBs), all sister spines contacting a MSB displayed a similar PSD area versus spine volume relationship (Figure 4.14 B).

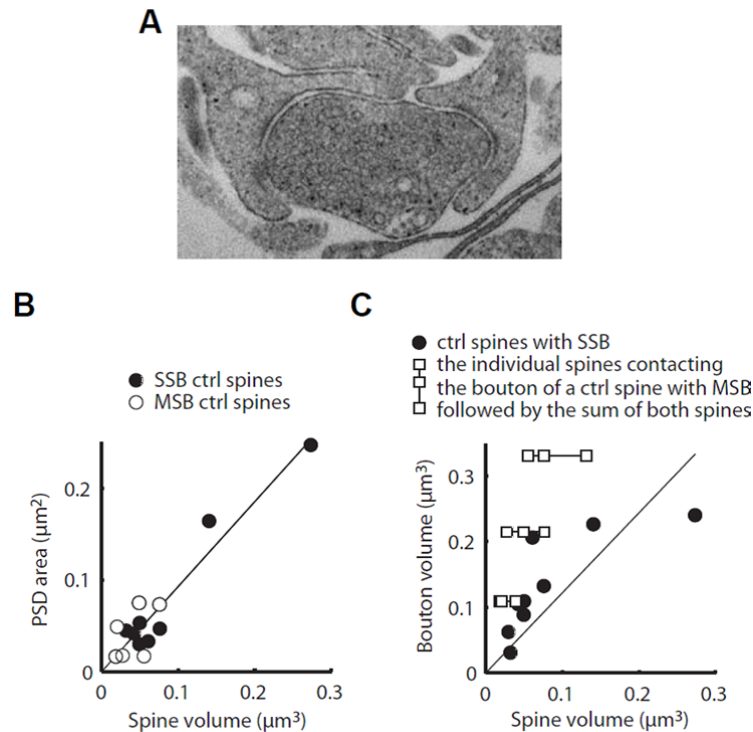


Figure 4.14: Characteristics of SSB and MSB synaptic contacts.

(A) EM image of a multi-synapse bouton contacting two spines.

(B) PSD area versus spine volume for SSB control spines (filled circles) and for MSB control spines (open circles), demonstrating a similar PSD area versus spine volume relationship for SSB and MSB spines. Line: linear fit to SSB data.

(C) Bouton volume versus spine volume for SSB control spines (circles) and for MSB control spines (squares): first two squares from the left represent the two individual spines of a MSB, and the last square the sum of both spines. The figure demonstrates that the bouton volume correlates better with the sum of the volume of its individual spines rather than with the volume of one particular spine. Therefore a share of the absolute bouton volume can be allocated to a spine of interest, leading to the relative bouton volume shown in Figure 4.15 B. Line: linear fit to SSB data.

In addition, with respect to the MSB volume, none of the individual spine volumes of spines contacting MSBs but the sum of their volumes matched the bouton volume / spine volume relationship of SSB spines (Figure 4.14 C).

Taken together, this suggests that there is no obvious structural interference between sister spines of MSBs and each can be assigned a share of the MSB volume according to their relative size. Using this procedure for MSBs, I pooled the data from single- and multi-synapse boutons.

4.5.2 Spine, PSD and bouton size correlate 3 hours after stimulation

In the following I describe the actual results obtained from my EM reconstructions. In this paragraph stimulated spines are defined as spines which 3 hours after stimulation were clearly increased in volume ($\geq 69\%$, mean, $130 \pm 18\%$, $n = 7$ spines / 7 cells), unless otherwise stated. As expected from our time-lapse recordings with labelled PSD proteins, I found that 3 hours after stimulation the relationship between PSD and spine size is not different in stimulated and control spines (mean ratio of PSD size over spine volume, control spines, $0.97 \pm 0.09 \mu\text{m}^{-1}$, $n = 11$ spines / 3 cells, stimulated spines, $1.06 \pm 0.16 \mu\text{m}^{-1}$, $n = 7$ spines / 7 cells; $p = 0.620$, two-tailed t-test) (Figure 4.15 A and C). It is unlikely that the enlargement of stimulated spines was not sufficiently strong to be accompanied by a significant increase in PSD size: From the final spine volume in the post-hoc ultrastructural reconstruction and the degree a given spine increased in size from the time-lapse imaging before and after stimulation, I can estimate its original volume. When then comparing stimulated spines with control spines which had volumes in the range of the initial volumes of stimulated spines (marked by the left end of the dashed lines in Figure 4.15 A and B), a significant difference in PSD size is obtained (selected control spines, $0.05 \pm 0.01 \mu\text{m}^2$, $n = 5$ spines / 2 cells; stimulated spines, $0.09 \pm 0.01 \mu\text{m}^2$, $n = 7$ spines / 7 cells; $p = 2.8 \cdot 10^{-4}$, one-tailed t-test) (Figure 4.15 D). In addition to the stimulated and stabilized spines I reconstructed one spine which did not show a persistent enlargement after stimulation: also here spine volume and PSD size correlated well (Figure 4.15 A). In summary, these results support the idea that the stabilization of synaptic modifications is linked to a parallel increase of spine and PSD.

As for PSD and spine size, I found that 3 hours after stimulation the relationship between bouton and spine volume is not different for stimulated and control spines (mean ratio of bouton over spine volume, control spines, 2.11 ± 0.22 , $n = 12$ spines / 3 cells, stimulated spines, 1.70 ± 0.30 , $n = 7$ spines / 7 cells; $p = 0.281$, two-tailed t-test) (Figure 4.15 B and C).

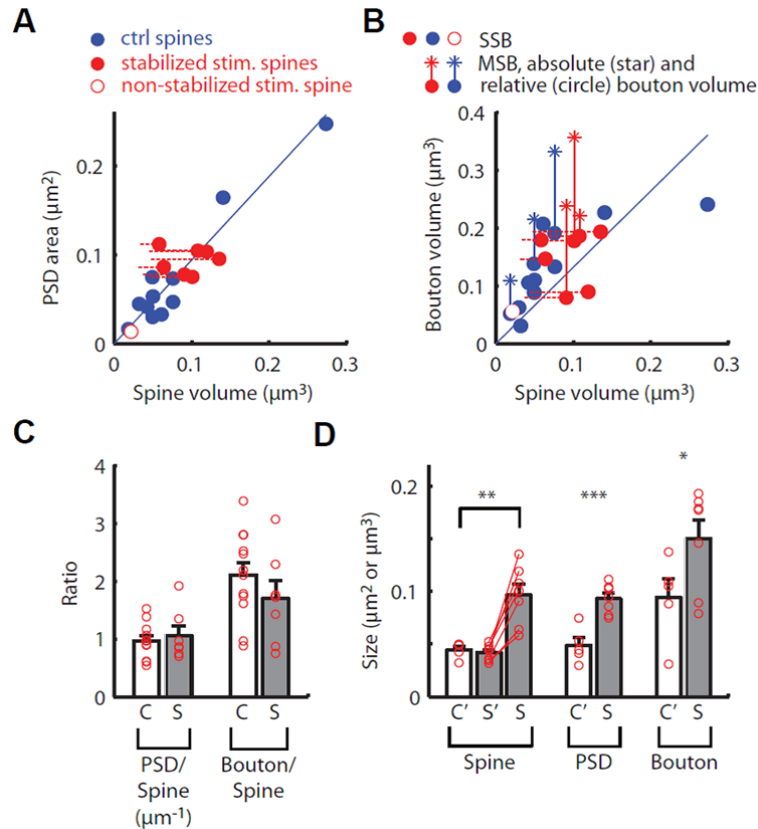


Figure 4.15: Electron microscopy of potentiated spines confirms PSD increase and reveals increase of bouton volume.

(A) PSD area plotted versus spine volume for stimulated spines (red) and control spines (blue). Blue line: linear fit to control data. Left end of red dashed lines indicates estimated spine volume before stimulation.

(B) As in (A) but for bouton and spine volume. Stars (absolute bouton volume) connected to filled circles (relative bouton volume, see main text for explanation) represent boutons which have more than one synaptic contact (multi-synapse bouton, MSB). SSB: single-synapse bouton.

(C) Ratios of PSD over spine volume and bouton over spine volume for data in (A,B). C = control spines, S = stimulated stabilized spines. Circles: Data for individual spines. Bars: mean value of ratios (PSD area, control, $n = 11$ spines / 3 cells, stimulated, $n = 7$ spines / 7 cells; bouton volume, control, $n = 12$ spines / 3 cells, stimulated, $n = 7$ spines / 7 cells; error bars, SEM).

(D) Spine, PSD and bouton size for control and stimulated stabilized spines. C' = selected control spines, S' = estimated spine volume before stimulation for stimulated stabilized spines, S = stimulated stabilized spines. Circles: Data for individual spines. Bars: mean; error bars, SEM. For control spines only those spines were chosen which displayed a volume in the range of the estimated spine volumes of stimulated spines before stimulation (stimulated spines, $n = 7$ spines / 7 cells; control spines, $n = 5$ spines / 2 cells). Stars indicate significance: * = $p < 0.05$, one-tailed t-test ; ** = $p < 0.01$, Wilcoxon rank sum test; *** = $p < 0.001$, one-tailed t-test).

This suggests that also the boutons associated with stimulated spines increased in size. Indeed, comparison of stimulated spines and control spines with volumes in the range of the original volumes of stimulated spines yields a significant difference in bouton volume (selected control spines, $0.09 \pm 0.02 \mu\text{m}^2$, $n = 5$ spines / 2 cells, stimulated spines, $0.15 \pm 0.02 \mu\text{m}^2$, $n = 7$ spines / 7 cells; $p = 0.029$, one-tailed t-test) (Figure 4.15 D). Last, in the spine which did not show a persistent enlargement, the bouton volume also correlated well with spine size, as the PSD did (Figure 4.15 B).

In conclusion, these results indicate that also at the ultrastructural level the correlation between spine, PSD and bouton size is maintained, both at persistently and non-persistently enlarged spines. Moreover, the hypothesis is further supported, that the stabilization of synaptic modifications requires parallel changes in all synaptic structures.

5. Discussion

Neuronal plasticity, i.e. activity dependent modification of neural networks, is considered to be the basis for learning and memory. Synaptic plasticity in particular describes a change in the connectivity of neurons or in the strength of synaptic transmission. Early EM studies demonstrated that synaptic structures, i.e. the spine, the postsynaptic density (PSD), the active zone (AZ) and the bouton correlate in size and with synaptic strength. During synaptic plasticity it is therefore expected that all synaptic structures undergo appropriate structural modifications, so that the correlation between the size of synaptic structures is reestablished and ultimately maintained. For example, during long-term potentiation (LTP) all synaptic structures should increase along with synaptic strength.

Functional changes indeed go in hand with structural changes (Desmond et al., 1983; Desmond et al., 1986; Desmond et al., 1988; Matsuzaki et al., 2004), but so far little is known about the detailed time course of alterations in synaptic structures during plasticity, in particular at the level of single spines. Furthermore, while the molecular mechanisms underlying functional and structural changes of synaptic contacts are relatively well studied, the processes leading to the stabilization of plasticity induced modifications are still not completely understood.

In my thesis I explored structural plasticity of individual spines and the stabilization of plasticity in more detail. Because glutamate uncaging allows for the induction of plasticity at single spines, I used this method to study postsynaptically induced structural modifications at CA3-CA1 Schaffer collateral synapses. In particular, I examined two hypotheses: First, together with the spine volume the other synaptic structures, in particular the PSD and presynaptic bouton, enlarge during synaptic potentiation. Second, the balancing of the synaptic structures is a signature for the stabilization of structural modifications. To explore these hypotheses, I used two different complementary approaches: First, I induced plasticity at single spines by two-photon glutamate uncaging, and performed time-lapse studies on changes in the amount of the PSD scaffolding proteins PSD-95 and Homer1c, which are good reporters for the size of the PSD due to their abundance and important functions within it. In the second approach, I reconstructed synaptic structures (spine, PSD, bouton) from electron micrographs of stimulated synapses 3 hours after glutamate uncaging.

I found that 3 hours after stimulation PSD-95 and Homer1c were increased in spines with persistent enlargement, but not in spines with non-stabilized volume increase. Furthermore, the correlation between PSD-95 or Homer1c levels with spine volume was maintained at 3 hours after stimulation. Also the EM reconstructions revealed that the naïve correlation between the size of the PSD and spine volume was maintained at 3 hours after stimulation in enlarged spines. Therefore both, important PSD scaffolding proteins and the PSD as an entity, increased during synaptic plasticity along with spine volume. In addition, EM analysis revealed that also bouton volumes were correlated with spine volume after stimulation. This is strong support for the hypothesis that the concomitant increase of all synaptic structures is a signature for the stabilization of synaptic modifications.

In the following, I will discuss the individual results of my thesis work in more detail.

5.1 PSD-95 and Homer1c are appropriate marker proteins for the PSD

To perform time-lapse studies on changes in spine volume and the PSD, I labelled the morphology of pyramidal cells by expressing the synaptic marker tdTomato, and co-expressed the PSD scaffolding proteins PSD-95 or Homer1c tagged with EGFP. Both PSD-95 and Homer1c were also used in other studies to explore synaptic plasticity or its underlying molecular mechanisms (Gray et al., 2006; Steiner et al., 2008; Petrini et al., 2009). The PSD marker proteins clearly localized to dendritic spines, although a minor fraction also was found in the dendrite. Therefore the measured PSD marker signal in the spine had to be corrected for the cytosolic signal.

Before setting up the actual experiments to explore correlated changes in synaptic structures, it was crucial to determine whether the overexpression of the PSD marker proteins might have any unwanted impact on my model system with respect to plasticity induction and maintenance. Therefore, I analyzed the spine volume of cells expressing only tdTomato, tdTomato + PSD-95-EGFP or tdTomato + EGFP-Homer1c. The determined spine volumes differed only negligibly from each other, in contrast to the results from Nikonenko et al. (Nikonenko et al., 2008), who demonstrated a more than twofold increase of spine volume in cells overexpressing PSD-95. Furthermore, Nikonenko found a

dramatically increased number of multi-innervated spines. However, these rather extreme effects might strongly depend on the amount of overexpressed PSD-95. I assume that in my experiments the expression of PSD-95 was low enough to not dramatically alter spine morphology. Interestingly, Homer1c expressing cells exhibited on average even slightly smaller spines compared to cells expressing only tdTomato. This finding is in accordance with the results described by Sala et al. (Sala et al., 2001).

Next, I ensured that the overexpression of the PSD marker proteins did not have a significant effect on the spine growth rate after plasticity induction. I found that, regardless of the type of protein expressed, the increase in spine volume was similar both immediately after and 1 hour after stimulation. This is similar to reports by Steiner et al. (Steiner et al., 2008) and stands in contrast to the findings by Stein et al. (Stein et al., 2003), who reported that the overexpression of PSD-95 occludes LTP. However, also here the effects of PSD-95 might strongly depend on the amount of overexpressed PSD-95, and on the exact experimental conditions such as temperature (35 °C in my experiments in contrast to RT in the work published by Stein et al.).

5.2 Correlation of PSD marker proteins with spine volume under naïve conditions

After having excluded potential unwanted side effects of PSD-95 or Homer1c overexpression on the induction and maintenance of plasticity related modifications, I set out to confirm whether PSD-95 and Homer1c indeed serve as good marker proteins for the size of the PSD (e.g. compare Sheng et al., 2007). If so, they should correlate with the spine volume in a similar way as it was shown for the PSD in electron microscopical studies (e.g. Schikorski et al., 1997; Arellano et al., 2007). Indeed I found that both proteins correlated well with spine volume.

Interestingly, Homer1c showed a tighter correlation with spine volume compared to PSD-95. This fact might be due to the more cytoplasmic localization of Homer1c within the PSD and its closer neighbourhood to actin (Ehlers, 2002): The cytoplasmic localization of Homer1c might allow for fast insertion or removal of Homer1c molecules. And the closer neighbourhood of Homer1c to actin might tightly link the number of Homer1c copies to the size of the spine, since actin is directly regulating spine volume changes.

5.3 Increase of PSD marker proteins along with spine volume during plasticity

After having established that PSD-95 and Homer1c represent appropriate marker proteins of the PSD, I was able to study modifications in the size of the PSD during structural plasticity in single dendritic spines. I did this by recording changes in the levels of PSD-95 and Homer1c. I found that on average both proteins increased over a time course of 3 hours after stimulation, however, PSD-95 increased in a delayed manner compared to the spine volume. This is in accordance with reports from Steiner et al. (Steiner et al., 2008) who did not find a significant increase in PSD-95 within the first 30 minutes after stimulation, either. Furthermore, I found that in control experiments the level of PSD-95 even decreased over time. Therefore, the increase of PSD-95 in stimulated spines can be corrected for this decrease.

Why does the kinetics of protein increase differ between PSD-95 and Homer1c? This difference between PSD-95 and Homer1c might reflect the slower turnover rate of PSD-95 compared to Homer1c (Kuriu et al., 2006), their different laminar positions within the PSD, where PSD-95 is found at the membrane face and Homer1c at the cytoplasmic face (Valtschanoff et al., 2001; Petralia et al., 2005), their interactions with different binding partners and the strength of these interactions (Kuriu et al., 2006), as well as their different signalling functions in the PSD (e.g. Inoue et al., 2007; Steiner et al., 2008). Furthermore, the increase in PSD-95 does not have to be fast, because synaptic strengthening, which occurs rapidly after stimulation, not necessarily has to be promoted by an increase in the number of AMPA receptor placeholders (which are provided by PSD-95), but might also be achieved by the incorporation of AMPA receptors at still unoccupied placeholders, or by a change in the activity of the receptors themselves. For example, it is possible that the initial phase of LTP is established via phosphorylation of AMPA receptor subunits, but is independent of AMPA receptor incorporation (Barria et al., 1997; Lee et al., 2000; Ehrlich et al., 2004, but also see Malenka, 2003). However, the reason for a delayed PSD-95 increase might also be found in the molecular pathways leading to PSD-95 incorporation into the PSD. It was shown that palmitoylation (Topinka et al., 1998; Craven et al., 1999) and phosphorylation (Kim et al., 2007) are crucial for the incorporation of PSD-95 into the PSD. Palmitoylation of PSD-95 is facilitated by the BDNF-PI3K-AKT and PKMzeta signalling pathways (Yoshii et al., 2011), and also depends on NMDA

receptor activation (Kolarow et al., 2007). Release of BDNF promotes the stabilization of spine enlargement (Tanaka et al., 2008) and induces transport of PSD-95 to dendrites and spines (Yoshii et al., 2007). Therefore, the delay in PSD-95 increase might be due to the time needed for the complex signalling processes (compare to the slow turnover rate of PSD-95 described above) to trigger PSD-95 incorporation, and these processes might at least in part depend on protein synthesis. Another possible explanation for the delayed increase of PSD-95 might be found in overexpression effects of PSD-95. Because the overexpression of PSD-95 did not have a strong impact on spine volume or plasticity induction in my experiments, I consider such overexpression effects as rather unlikely. Nevertheless, it might be possible that overexpression leads to a strong enrichment of PSD-95 within the PSD (e.g. compare to Nikonenko et al., 2008, who showed that PSD-95 overexpression leads to an enlarged PSD). Therefore the increase of PSD-95 to promote synaptic strengthening in stimulated spines might be delayed, because preexistent PSD-95 molecules could prevent the incorporation of new PSD-95 molecules.

The observation that PSD-95 level decrease in control spines over time might be explained by results from Zhang and Lisman (Zhang et al., 2011): They report that the application of TTX leads to a significant decrease of PSD-95 level. Therefore, in my experiments activity blockage by TTX might account for the decrease in PSD-95.

5.4 Reestablishment of the correlation between PSD size and spine volume

Over a period of 3 hours after stimulation the amount of PSD marker proteins and spine volume moved towards a new balance at a larger overall size, and the naïve correlation between PSD size and spine volume was reestablished. This reestablishment needed some time, because 1 hour after stimulation the naïve correlation was still disrupted in case of PSD-95, due to its delayed increase as discussed above. The balancing of PSD size and spine volume was expected from the existence of the naïve correlation between these structures, but now the time course of this readjustment was demonstrated for the first time on the level of single spines. Furthermore, because changes in PSD-95 and Homer1c levels displayed different kinetics, one can conclude that the rearrangement of the PSD as a whole does not occur at once. The mechanisms underlying the

increase of the PSD are most likely complex, and depend on the interaction between the multitude of proteins which form the dense meshwork of the PSD structure. In particular, the interplay between actin, different signalling molecules such as Rho GTPases, and scaffolding proteins like PSD-95, Homer1c and Shank might be involved in the PSD's enlargement, which is likely to be a cooperative process (Eccles, 1983; Shepherd et al., 2011) in a molecular crowding environment (Ellis, 2001; Santamaria et al., 2010). It remains interesting to solve this puzzle of interactions and to elaborate a model of the single molecular pathways leading to structural changes in the spine and the PSD.

5.5 Stabilization of structural modifications

My experiments demonstrated that in general the correlation between PSD marker proteins and spine volume is reestablished 3 hours after stimulation. Next, I was interested in whether this reestablishment is connected to the stabilization of structural modifications. Therefore I separated the data into two different groups, namely spines with a strong persistent enlargement (stabilized spines) and spines with non-persistent enlargement (non-stabilized spines). In the first group, PSD-95 increased slowly over time, and Homer1c level increased within 20 minutes after stimulation. In contrast, in the group of non-stabilized spines, PSD-95 level did not increase and Homer1c level increased only transiently. From this result one can infer that the parallel increase of both spine volume and PSD is a signature for the stabilization of structural modifications in spines during plasticity.

Interestingly, my observations regarding the increase of PSD marker proteins resemble the different phases of LTP establishment: First, within a short time window after induction of plasticity (approximately during the first 15-30 minutes), LTP is subject to reversal by low frequency stimulation (Staubli et al., 1999). Notably, Homer1c increases during that time and reaches its plateau 20 minutes after stimulation. This time point might mark the onset of intermediate stabilization of LTP. The second phase, also referred to as early LTP (E-LTP), is defined by its independence of protein synthesis, and lasts for about 1 hour after stimulation (Redondo et al., 2011). After that time E-LTP decays. Around the same time I found that the spine volume of non-stabilized spines started to decrease. The last phase, known as late LTP (L-LTP), ultimately defines a condition of enduring potentiation which persists over extended time, and

which is dependent on protein synthesis (Redondo et al., 2011). In my experiments, the time needed for the increase in PSD-95 to match the spine volume enlargement falls into this last phase of LTP. Therefore, and because the increase of PSD-95 might be protein synthesis dependent (compare section 5.3), the increase in PSD-95 might be a hallmark of L-LTP.

5.6 Forskolin and the stabilization of structural modifications

After having studied modifications in spine volume and PSD structure during plasticity without pharmacological alteration of the system, I was interested in whether pharmacological promotion or stabilization of structural changes might accelerate the increase in PSD-95 during plasticity. Therefore I applied the PKA activator forskolin, which was shown to lead to an increased spine enlargement after glutamate uncaging, and it supports the stabilization of structural modifications during plasticity (Govindarajan et al., 2011).

However, when applying forskolin I obtained unexpected results: the overall increase in spine volume at 3 hours after stimulation was not enhanced, the ratio of stabilized versus non-stabilized spines did not change, and the PSD-95 level did not increase significantly earlier or stronger compared to experiments without forskolin.

I can only speculate about the reason for these unexpected results: Because in forskolin control experiments PSD-95 level did not decrease compared to experiments without forskolin, this speaks for a role of forskolin in regulating global plasticity-related modifications rather than having a spine specific effect. In my experiments activity was blocked by TTX (in contrast to Govindarajan et al.), therefore the global effect of forskolin might not be established, and therefore also at the level of single spines the promoting and stabilizing effects of forskolin on spine growth might be occluded or prevented. Furthermore, also the overexpression of PSD-95, even though rather low in my experiments, might diminish the forskolin effects, due to an overall increase of PSD-95 in spines.

5.7 Correlation of spine, PSD and bouton size in EM reconstructions

By two-photon time-lapse imaging I demonstrated that plasticity induction at single spines leads to both an enlargement in spine volume and an increase in the PSD marker proteins PSD-95 and Homer1c. However, despite their abundance

and their important functions within the postsynaptic density, Homer1c and PSD-95 represent only two out of the multitude of proteins which form the PSD. Thus, an increase in these two proteins does not necessarily represent an enlargement of the PSD as a structural entity. Therefore, in a second experimental approach, I stimulated single spines by glutamate uncaging, imaged them for 3 hours, and subsequently analyzed the synapses associated with these spines by reconstruction of spine, PSD and bouton using electron microscopy. Before interpreting the results, I discuss some specific observations in my EM experiments:

Many of the analyzed boutons contained a high number of synaptic vesicles, and some boutons were even completely filled with these. In a few cases the distribution of the vesicles even extended beyond the boutons into the axons. Therefore it was not possible to use the number of membrane-attached vesicles as measure for presynaptic strength, because the vesicles touched the membrane all along the bouton surface. In the literature I found different EM images of boutons, in some of them the boutons contained many vesicles, but in others they did not (e.g. Desmond et al., 1983; Desmond et al., 1986; Schikorski et al., 1997; Harris et al., 2012). I speculate that the concrete slice culturing conditions play a role, or that the shrinkage of tissue during fixation leads to an increased density of vesicles. Last, but rather unlikely, the presence of TTX in my experiments might lead to an increase in the number of vesicles due to synaptic scaling. However, such homeostatic effects are known to occur after a far longer period of time, lasting over several days (Murthy et al., 2001).

Furthermore, I observed that some of the reconstructed synapses displayed multi-synapse boutons (MSBs), which make contacts to several spines. This seems to be nothing unusual: it was shown that large boutons frequently exhibit multiple synaptic contacts (Holtmaat et al., 2009), and most of the MSBs in my experiments indeed had rather large volumes.

After having described these observations, I now want to discuss the structural plasticity-related results of my EM experiments: I found that 3 hours after stimulation the correlation between PSD and spine size as well as between bouton and spine volume matched the respective naïve correlation at control spines. This was true for both stabilized spines and a single non-stabilized spine. In the case of stabilized spines, the increase in spine volume was strong enough to exclude the possibility that the correlation might have been maintained without any increase of the PSD or bouton. Therefore, it can be concluded that

both the PSD and bouton increased at the latest within 3 hours after stimulation on the level of a single spine. Because for both the stabilized spines and for the single non-stabilized spine the correlation between synaptic structures remained unchanged on the long term, the hypothesis is further supported that the reestablishment of the correlation between synaptic structures is a signature for the stabilization of structural modifications.

With these experiments, I demonstrated correlated changes in complete synaptic structures for the first time on the level of single synapses, and in general for the first time for boutons. So far, modifications in the spine and the PSD were only shown at the population level by electron microscopy after LTP induction, and the observed results were inconsistent (Desmond et al., 1983; Desmond et al., 1986; Desmond et al., 1988; Sorra et al., 1998). Interestingly, Desmond reported that the PSD may increase already within 2 minutes after LTP induction (Desmond et al., 1986). Therefore, also on the level of a single synapse, the PSD as entity might increase already far earlier than within the 3 hours after stimulation as shown in my EM experiments.

The fact that besides the spine and PSD also the boutons increased in volume can be either explained by activation of presynaptic glutamate receptors during uncaging (e.g. presynaptic NMDA receptors, McGuinness et al., 2010), or by the involvement of a retrograde transsynaptic signalling mechanism from the spine to the presynapse (Malenka et al., 2004; Dalva et al., 2007; Enoki et al., 2009; Regehr et al., 2009; Castillo, 2012).

6. Conclusions and Outlook

The goal of my thesis was to demonstrate that on the level of a single synapse the correlation between synaptic structures, as seen in ultrastructural reconstructions, is maintained or reestablished during synaptic plasticity by parallel enlargement of spine, PSD and bouton. Furthermore, I wanted to explore the hypothesis that the balancing of these synaptic structures is a signature for the stabilization of structural modifications. Indeed, I could show that 3 hours after stimulation of a single dendritic spine two major scaffolding proteins of the PSD, namely PSD-95 and Homer1c, were increased in spines with persistent enlargement, but not in transiently growing spines. Whereas Homer1c increased immediately after stimulation, the increase in PSD-95 occurred with a delay. In addition, ultrastructural reconstruction of spine, PSD and bouton revealed an increase of all these structures within 3 hours after stimulation. Since the PSD as such is a complex of multiple proteins, the time course of enlargement of the PSD as an entity and the rearrangement of its individual molecular components do not necessarily have to match. Nonetheless, upon completion of the rearrangement of the PSD one would expect that by addition of appropriate numbers of protein modules the equilibrium composition of the PSD is reestablished, which was the case for PSD-95 and Homer1c.

The pre- and postsynaptic compartment might be considered as large supramolecular complexes at which the correlation of synaptic structures results from the mutual stabilization of structural proteins. In such a supramolecular complex the multitude and possibly redundancy of interactions might provide comprehensive structural stability despite comparatively fast turnover of the single constituting molecular components. In this sense, the structural correlation might be regarded as a form of memory engram for the size and strength of the synapse.

In conclusion, my data support my initial hypotheses, and suggest a model of synaptic plasticity where correlated rearrangement of post- and presynaptic structures stabilizes synaptic potentiation (Figure 6.1).

My experiments demonstrated that spine, PSD and bouton increase within a time frame of 3 hours along with synaptic strength during single synapse plasticity. However, at present we still just understand a fraction of the complex molecular machinery which constitutes the driving force of the structural and functional remodelling of synapses. Therefore, it remains interesting to study the

biochemical foundations of synaptic plasticity in much greater detail and to solve the molecular puzzle which empowers our brain to perform such outstanding tasks like to adapt, to learn and to memorize.

For example, the ultrastructural analysis of stimulated spines allowed for determining the size of the PSD as an entity. However, the term “entity” refers to the structural dimensions of the PSD, but not to its single molecular constituents. This means that still only little can be said about the changes in individual components of the PSD during spine plasticity, apart from PSD-95 and Homer1c. Furthermore, understanding the retrograde signalling mechanisms relaying postsynaptic modifications to the presynapse is of keen interest. In addition, also the structural modifications and molecular processes occurring at the active zone as well as at other synaptic contacts apart from the CA3-CA1 Schaffer collateral synapse remain to be explored.

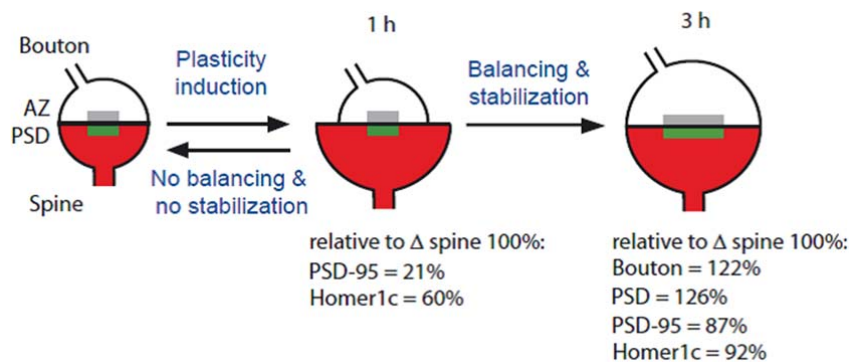


Figure 6.1: Final model illustrating the relationship between the stabilization of synapse enlargement during structural plasticity and the correlation in the dimensions of synaptic structures.

Postsynaptic stimulation leads to an increase of spine volume. If subsequently PSD, bouton and most likely also the active zone (AZ) increase such that the morphological correlations are reestablished, then the synaptic structures become stabilized at the enlarged size. However, if the other synaptic structures fail to increase, then the morphological correlations are reestablished by a reversion of the spine enlargement and the synapse decays to its initial size. The displayed values are the mean changes in PSD-95 and Homer1c level at 1 hour (time bin 45-75 minutes after stimulation) and 3 hours after stimulation (last time bin), normalized to a spine volume increase of 100%. The values for PSD and bouton increase were estimated from our EM data by comparing the ratios of PSD / spine size and bouton / spine size between stimulated and control spines, under consideration of the spine growth rate obtained from two-photon imaging.

7. References

- Abel T. and P. V. Nguyen** (2008). "Regulation of hippocampus-dependent memory by cyclic AMP-dependent protein kinase." *Prog Brain Res* **169**, 97-115.
- Abel T., P. V. Nguyen, M. Barad, T. A. Deuel, E. R. Kandel and R. Bourtchouladze** (1997). "Genetic demonstration of a role for PKA in the late phase of LTP and in hippocampus-based long-term memory." *Cell* **88**(5), 615-26.
- Abraham W. C. and J. M. Williams** (2003). "Properties and mechanisms of LTP maintenance." *Neuroscientist* **9**(6), 463-74.
- Arellano J. I., R. Benavides-Piccione, J. Defelipe and R. Yuste** (2007). "Ultrastructure of dendritic spines: correlation between synaptic and spine morphologies." *Front Neurosci* **1**(1), 131-43.
- Barria A., D. Muller, V. Derkach, L. C. Griffith and T. R. Soderling** (1997). "Regulatory phosphorylation of AMPA-type glutamate receptors by CaM-KII during long-term potentiation." *Science* **276**(5321), 2042-5.
- Beique J. C. and R. Andrade** (2003). "PSD-95 regulates synaptic transmission and plasticity in rat cerebral cortex." *J Physiol* **546**(Pt 3), 859-67.
- Bishop D., I. Nikić, M. Brinkoetter, S. Knecht, S. Potz, M. Kerschensteiner and T. Misgeld** (2011). "Near-infrared branding efficiently correlates light and electron microscopy." *Nat Methods* **8**(7), 568-70.
- Blanpied T. A., J. M. Kerr and M. D. Ehlers** (2008). "Structural plasticity with preserved topology in the postsynaptic protein network." *Proc Natl Acad Sci U S A* **105**(34), 12587-92.
- Bliss T. V. P. and T. Lomo** (1973). "Long-lasting potentiation of synaptic transmission in the dentate area of the anaesthetized rabbit following stimulation of the perforant path." *The Journal of Physiology Online* **232**(2), 331-356.
- Bozdagi O., W. Shan, H. Tanaka, D. L. Benson and G. W. Huntley** (2000). "Increasing numbers of synaptic puncta during late-phase LTP: N-cadherin is synthesized, recruited to synaptic sites, and required for potentiation." *Neuron* **28**(1), 245-59.

- Bozdagi O., X. B. Wang, J. S. Nikitczuk, T. R. Anderson, E. B. Bloss, G. L. Radice, Q. Zhou, D. L. Benson and G. W. Huntley** (2010). "Persistence of coordinated long-term potentiation and dendritic spine enlargement at mature hippocampal CA1 synapses requires N-cadherin." *Journal of Neuroscience* **30**(30), 9984-9989.
- Bredt D. S. and R. A. Nicoll** (2003). "AMPA receptor trafficking at excitatory synapses." *Neuron* **40**(2), 361-79.
- Castillo P. E.** (2012). "Presynaptic LTP and LTD of excitatory and inhibitory synapses." *Cold Spring Harb Perspect Biol* **4**(2).
- Chen X., C. D. Nelson, X. Li, C. A. Winters, R. Azzam, A. A. Sousa, R. D. Leapman, H. Gainer, M. Sheng and T. S. Reese** (2011). "PSD-95 Is Required to Sustain the Molecular Organization of the Postsynaptic Density." *J Neurosci* **31**(17), 6329-6338.
- Chen X., C. Winters, R. Azzam, X. Li, J. A. Galbraith, R. D. Leapman and T. S. Reese** (2008). "Organization of the core structure of the postsynaptic density." *Proceedings of the National Academy of Sciences* **105**(11), 4453-4458.
- Chen Y. and B. L. Sabatini** (2012). "Signaling in dendritic spines and spine microdomains." *Curr Opin Neurobiol*.
- Cosgrove K. E., E. J. Galvan, G. Barrionuevo and S. D. Meriney** (2011). "mGluRs modulate strength and timing of excitatory transmission in hippocampal area CA3." *Mol Neurobiol* **44**(1), 93-101.
- Craven S. E., A. E. El-Husseini and D. S. Bredt** (1999). "Synaptic targeting of the postsynaptic density protein PSD-95 mediated by lipid and protein motifs." *Neuron* **22**(3), 497-509.
- Dalva M. B., A. C. McClelland and M. S. Kayser** (2007). "Cell adhesion molecules: signalling functions at the synapse." *Nat Rev Neurosci* **8**(3), 206-20.
- Denk W., J. H. Strickler and W. W. Webb** (1990). "Two-photon laser scanning fluorescence microscopy." *Science* **248**(4951), 73-6.
- Desmond N. L. and W. B. Levy** (1983). "Synaptic correlates of associative potentiation/depression: an ultrastructural study in the hippocampus." *Brain Res* **265**(1), 21-30.
- Desmond N. L. and W. B. Levy** (1986). "Changes in the postsynaptic density with long-term potentiation in the dentate gyrus." *J Comp Neurol* **253**(4), 476-82.

- Desmond N. L. and W. B. Levy** (1988). "Synaptic interface surface area increases with long-term potentiation in the hippocampal dentate gyrus." *Brain Res* **453**(1-2), 308-14.
- Eccles J. C.** (1983). "Calcium in long-term potentiation as a model for memory." *Neuroscience* **10**(4), 1071-81.
- Egea J. and R. Klein** (2007). "Bidirectional Eph-ephrin signaling during axon guidance." *Trends Cell Biol* **17**(5), 230-8.
- Ehlers M. D.** (2002). "Molecular morphogens for dendritic spines." *Trends Neurosci* **25**(2), 64-7.
- Ehrlich I., M. Klein, S. Rumpel and R. Malinow** (2007). "PSD-95 is required for activity-driven synapse stabilization." *Proc Natl Acad Sci U S A* **104**(10), 4176-81.
- Ehrlich I. and R. Malinow** (2004). "Postsynaptic density 95 controls AMPA receptor incorporation during long-term potentiation and experience-driven synaptic plasticity." *J Neurosci* **24**(4), 916-27.
- El-Husseini A. E.-D., E. Schnell, D. M. Chetkovich, R. A. Nicoll and D. S. Brecht** (2000). "PSD-95 Involvement in Maturation of Excitatory Synapses." *Science* **290**(5495), 1364-1368.
- Ellis R. J.** (2001). "Macromolecular crowding: obvious but underappreciated." *Trends Biochem Sci* **26**(10), 597-604.
- Engert F. and T. Bonhoeffer** (1999). "Dendritic spine changes associated with hippocampal long-term synaptic plasticity." *Nature* **399**(6731), 66-70.
- Enoki R., Y. L. Hu, D. Hamilton and A. Fine** (2009). "Expression of long-term plasticity at individual synapses in hippocampus is graded, bidirectional, and mainly presynaptic: optical quantal analysis." *Neuron* **62**(2), 242-53.
- Fiala J. C.** (2005). "Reconstruct: a free editor for serial section microscopy." *J Microsc* **218**(Pt 1), 52-61.
- Frey U., Y. Y. Huang and E. R. Kandel** (1993). "Effects of cAMP simulate a late stage of LTP in hippocampal CA1 neurons." *Science* **260**(5114), 1661-4.
- Frey U. and R. G. Morris** (1998). "Synaptic tagging: implications for late maintenance of hippocampal long-term potentiation." *Trends Neurosci* **21**(5), 181-8.

- Futai K., M. J. Kim, T. Hashikawa, P. Scheiffele, M. Sheng and Y. Hayashi** (2007). "Retrograde modulation of presynaptic release probability through signaling mediated by PSD-95-neurologin." *Nat Neurosci* **10**(2), 186-195.
- Govindarajan A., I. Israely, S. Y. Huang and S. Tonegawa** (2011). "The dendritic branch is the preferred integrative unit for protein synthesis-dependent LTP." *Neuron* **69**(1), 132-46.
- Gray N. W., R. M. Weimer, I. Bureau and K. Svoboda** (2006). "Rapid redistribution of synaptic PSD-95 in the neocortex in vivo." *PLoS.Biol.* **4**(11), e370.
- Grunwald I. C., M. Korte, G. Adelman, A. Plueck, K. Kullander, R. H. Adams, M. Frotscher, T. Bonhoeffer and R. Klein** (2004). "Hippocampal plasticity requires postsynaptic ephrinBs." *Nat Neurosci* **7**(1), 33-40.
- Gundelfinger E. D. and A. Fejtova** (2012). "Molecular organization and plasticity of the cytomatrix at the active zone." *Curr Opin Neurobiol* **22**(3), 423-30.
- Harris K. M. and J. K. Stevens** (1989). "Dendritic spines of CA 1 pyramidal cells in the rat hippocampus: serial electron microscopy with reference to their biophysical characteristics." *Journal of Neuroscience* **9**(8), 2982-2997.
- Harris K. M. and R. J. Weinberg** (2012). "Ultrastructure of Synapses in the Mammalian Brain." *Cold Spring Harb Perspect Biol.*
- Harvey C. D. and K. Svoboda** (2007). "Locally dynamic synaptic learning rules in pyramidal neuron dendrites." *Nature* **450**(7173), 1195-1200.
- Harvey C. D., R. Yasuda, H. Zhong and K. Svoboda** (2008). "The spread of Ras activity triggered by activation of a single dendritic spine." *Science* **321**(5885), 136-40.
- Hayashi M. K., H. M. Ames and Y. Hayashi** (2006). "Tetrameric hub structure of postsynaptic scaffolding protein homer." *J Neurosci* **26**(33), 8492-501.
- Hayashi M. K., C. Tang, C. Verpelli, R. Narayanan, M. H. Stearns, R. M. Xu, H. Li, C. Sala and Y. Hayashi** (2009). "The postsynaptic density proteins Homer and Shank form a polymeric network structure." *Cell* **137**(1), 159-71.
- Hebb D. O.** (1949). "A neuropsychological theory." New York, *Wiley*.
- Hering H. and M. Sheng** (2001). "Dendritic spines: structure, dynamics and regulation." *Nat Rev Neurosci* **2**(12), 880-8.

- Holderith N., A. Lorincz, G. Katona, B. Rozsa, A. Kulik, M. Watanabe and Z. Nusser** (2012). "Release probability of hippocampal glutamatergic terminals scales with the size of the active zone." *Nat Neurosci* **15**(7), 988-997.
- Holtmaat A. and K. Svoboda** (2009). "Experience-dependent structural synaptic plasticity in the mammalian brain." *Nat Rev Neurosci* **10**(9), 647-58.
- Honkura N., M. Matsuzaki, J. Noguchi, G. C. Ellis-Davies and H. Kasai** (2008). "The subspine organization of actin fibers regulates the structure and plasticity of dendritic spines." *Neuron* **57**(5), 719-29.
- Hosokawa T., D. A. Rusakov, T. V. Bliss and A. Fine** (1995). "Repeated confocal imaging of individual dendritic spines in the living hippocampal slice: evidence for changes in length and orientation associated with chemically induced LTP." *J Neurosci* **15**(8), 5560-73.
- Inoue Y., H. Udo, K. Inokuchi and H. Sugiyama** (2007). "Homer1a regulates the activity-induced remodeling of synaptic structures in cultured hippocampal neurons." *Neuroscience* **150**(4), 841-852.
- Kim E. and M. Sheng** (2004). "PDZ domain proteins of synapses." *Nature Reviews Neuroscience* **5**(10), 771-781.
- Kim M. J., K. Futai, J. Jo, Y. Hayashi, K. Cho and M. Sheng** (2007). "Synaptic accumulation of PSD-95 and synaptic function regulated by phosphorylation of serine-295 of PSD-95." *Neuron* **56**(3), 488-502.
- Knott G. W., A. Holtmaat, J. T. Trachtenberg, K. Svoboda and E. Welker** (2009). "A protocol for preparing GFP-labeled neurons previously imaged in vivo and in slice preparations for light and electron microscopic analysis." *Nat Protoc* **4**(8), 1145-56.
- Kolarow R., T. Brigadski and V. Lessmann** (2007). "Postsynaptic secretion of BDNF and NT-3 from hippocampal neurons depends on calcium calmodulin kinase II signaling and proceeds via delayed fusion pore opening." *J Neurosci* **27**(39), 10350-64.
- Kopec C. D., E. Real, H. W. Kessels and R. Malinow** (2007). "GluR1 links structural and functional plasticity at excitatory synapses." *J Neurosci* **27**(50), 13706-18.
- Kramar E. A., B. Lin, C. S. Rex, C. M. Gall and G. Lynch** (2006). "Integrin-driven actin polymerization consolidates long-term potentiation." *Proceedings of the National Academy of Sciences* **103**(14), 5579-5584.

- Krucker T., G. R. Siggins and S. Halpain** (2000). "Dynamic actin filaments are required for stable long-term potentiation (LTP) in area CA1 of the hippocampus." *Proceedings of the National Academy of Sciences* **97**(12), 6856-6861.
- Kuczewski N., C. Porcher and J. L. Gaiarsa** (2010). "Activity-dependent dendritic secretion of brain-derived neurotrophic factor modulates synaptic plasticity." *Eur J Neurosci*.
- Kuriu T., A. Inoue, H. Bito, K. Sobue and S. Okabe** (2006). "Differential control of postsynaptic density scaffolds via actin-dependent and -independent mechanisms." *J Neurosci* **26**(29), 7693-706.
- Lee H. K., M. Barbarosie, K. Kameyama, M. F. Bear and R. L. Huganir** (2000). "Regulation of distinct AMPA receptor phosphorylation sites during bidirectional synaptic plasticity." *Nature* **405**(6789), 955-9.
- Lee S. J., Y. Escobedo-Lozoya, E. M. Szatmari and R. Yasuda** (2009). "Activation of CaMKII in single dendritic spines during long-term potentiation." *Nature* **458**(7236), 299-304.
- Lohmann C. and T. Bonhoeffer** (2008). "A role for local calcium signaling in rapid synaptic partner selection by dendritic filopodia." *Neuron* **59**(2), 253-60.
- Luscher C. and R. C. Malenka** (2012). "NMDA receptor-dependent long-term potentiation and long-term depression (LTP/LTD)." *Cold Spring Harb Perspect Biol* **4**(6).
- Malenka R. C.** (2003). "Synaptic plasticity and AMPA receptor trafficking." *Ann N Y Acad Sci* **1003**, 1-11.
- Malenka R. C. and M. F. Bear** (2004). "LTP and LTD: an embarrassment of riches." *Neuron* **44**(1), 5-21.
- Malenka R. C. and R. A. Nicoll** (1993). "NMDA-receptor-dependent synaptic plasticity: multiple forms and mechanisms." *Trends Neurosci* **16**(12), 521-7.
- Maletic-Savatic M., R. Malinow and K. Svoboda** (1999). "Rapid dendritic morphogenesis in CA1 hippocampal dendrites induced by synaptic activity." *Science* **283**(5409), 1923-7.
- Malinow R.** (2003). "AMPA receptor trafficking and long-term potentiation." *Philos Trans R Soc Lond B Biol Sci* **358**(1432), 707-14.

- Matsuzaki M., G. C. Ellis-Davies, T. Nemoto, Y. Miyashita, M. Iino and H. Kasai** (2001). "Dendritic spine geometry is critical for AMPA receptor expression in hippocampal CA1 pyramidal neurons." *Nat Neurosci* **4**(11), 1086-92.
- Matsuzaki M., N. Honkura, G. C. Ellis-Davies and H. Kasai** (2004). "Structural basis of long-term potentiation in single dendritic spines." *Nature* **429**(6993), 761-6.
- McAllister A. K.** (2000). "Biolistic transfection of neurons." *Sci STKE* **2000**(51), PL1.
- McGuinness L., C. Taylor, R. D. Taylor, C. Yau, T. Langenhan, M. L. Hart, H. Christian, P. W. Tynan, P. Donnelly and N. J. Emptage** (2010). "Presynaptic NMDARs in the hippocampus facilitate transmitter release at theta frequency." *Neuron* **68**(6), 1109-27.
- Mendez P., M. De Roo, L. Poglia, P. Klauser and D. Muller** (2010). "N-cadherin mediates plasticity-induced long-term spine stabilization." *J Cell Biol* **189**(3), 589-600.
- Murakoshi H., H. Wang and R. Yasuda** (2011). "Local, persistent activation of Rho GTPases during plasticity of single dendritic spines." *Nature* **472**(7341), 100-4.
- Murthy V. N., T. Schikorski, C. F. Stevens and Y. Zhu** (2001). "Inactivity Produces Increases in Neurotransmitter Release and Synapse Size." *Neuron* **32**(4), 673-682.
- Newpher T. M. and M. D. Ehlers** (2009). "Spine microdomains for postsynaptic signaling and plasticity." *Trends Cell Biol* **19**(5), 218-27.
- Nicoll R. A., S. Tomita and D. S. Brecht** (2006). "Auxiliary subunits assist AMPA-type glutamate receptors." *Science* **311**(5765), 1253-6.
- Nikonenko B. V., K. A. Sacksteder, S. Hundert, L. Einck and C. A. Nacy** (2008). "PSD-95 promotes synaptogenesis and multiinnervated spine formation through nitric oxide signaling." *J Cell Biol* **3**(2), 102-16.
- Nimchinsky E. A., B. L. Sabatini and K. Svoboda** (2002). "Structure and function of dendritic spines." *Annu Rev Physiol* **64**, 313-53.
- Okamoto K., T. Nagai, A. Miyawaki and Y. Hayashi** (2004). "Rapid and persistent modulation of actin dynamics regulates postsynaptic reorganization underlying bidirectional plasticity." *Nat Neurosci* **7**(10), 1104-12.

- Peters A. and I. R. Kaiserman-Abramof** (1970). "The small pyramidal neuron of the rat cerebral cortex. The perikaryon, dendrites and spines." *Am J Anat* **127**(4), 321-55.
- Petralia R. S., N. Sans, Y. X. Wang and R. J. Wenthold** (2005). "Ontogeny of postsynaptic density proteins at glutamatergic synapses." *Mol Cell Neurosci* **29**(3), 436-52.
- Petrini E. M., J. Lu, L. Cognet, B. Lounis, M. D. Ehlers and D. Choquet** (2009). "Endocytic trafficking and recycling maintain a pool of mobile surface AMPA receptors required for synaptic potentiation." *Neuron* **63**(1), 92-105.
- Redondo R. L. and R. G. Morris** (2011). "Making memories last: the synaptic tagging and capture hypothesis." *Nat Rev Neurosci* **12**(1), 17-30.
- Regalado M. P., R. T. Terry-Lorenzo, C. L. Waites, C. C. Garner and R. C. Malenka** (2006). "Transsynaptic signaling by postsynaptic synapse-associated protein 97." *J Neurosci* **26**(8), 2343-57.
- Regehr W. G., M. R. Carey and A. R. Best** (2009). "Activity-dependent regulation of synapses by retrograde messengers." *Neuron* **63**(2), 154-70.
- Sala C., V. Piech, N. R. Wilson, M. Passafaro, G. Liu and M. Sheng** (2001). "Regulation of dendritic spine morphology and synaptic function by Shank and Homer." *Neuron* **31**(1), 115-30.
- Santamaria F., J. Gonzalez, G. J. Augustine and S. Raghavachari** (2010). "Quantifying the effects of elastic collisions and non-covalent binding on glutamate receptor trafficking in the post-synaptic density." *PLoS Comput Biol* **6**(5), e1000780.
- Schikorski T. and C. F. Stevens** (1997). "Quantitative ultrastructural analysis of hippocampal excitatory synapses." *J Neurosci* **17**(15), 5858-67.
- Schikorski T. and C. F. Stevens** (1999). "Quantitative fine-structural analysis of olfactory cortical synapses." *Proc Natl Acad Sci U S A* **96**(7), 4107-12.
- Schoch S. and E. D. Gundelfinger** (2006). "Molecular organization of the presynaptic active zone." *Cell Tissue Res* **326**(2), 379-91.
- Sheng M. and C. C. Hoogenraad** (2007). "The postsynaptic architecture of excitatory synapses: a more quantitative view." *Annu Rev Biochem* **76**, 823-47.
- Sheng M. and C. Sala** (2001). "PDZ domains and the organization of supramolecular complexes." *Annu Rev Neurosci* **24**, 1-29.

- Shepherd G. M. and K. M. Harris** (1998). "Three-dimensional structure and composition of CA3-->CA1 axons in rat hippocampal slices: implications for presynaptic connectivity and compartmentalization." *J Neurosci* **18**(20), 8300-10.
- Shepherd T. R. and E. J. Fuentes** (2011). "Structural and thermodynamic analysis of PDZ-ligand interactions." *Methods Enzymol* **488**, 81-100.
- Shiraishi-Yamaguchi Y. and T. Furuichi** (2007). "The Homer family proteins." *Genome Biol* **8**(2), 206.
- Sobczyk A., V. Scheuss and K. Svoboda** (2005). "NMDA receptor subunit-dependent [Ca²⁺] signaling in individual hippocampal dendritic spines." *J Neurosci* **25**(26), 6037-46.
- Sorra K. E. and K. M. Harris** (1998). "Stability in synapse number and size at 2 hr after long-term potentiation in hippocampal area CA1." *J Neurosci* **18**(2), 658-71.
- Squire L. R. and S. Zola-Morgan** (1991). "The medial temporal lobe memory system." *Science* **253**(5026), 1380-6.
- Staubli U. and J. Scafidi** (1999). "Time-dependent reversal of long-term potentiation in area CA1 of the freely moving rat induced by theta pulse stimulation." *J Neurosci* **19**(19), 8712-9.
- Stein V., D. R. C. House, D. S. Bredt and R. A. Nicoll** (2003). "Postsynaptic Density-95 Mimics and Occludes Hippocampal Long-Term Potentiation and Enhances Long-Term Depression." *J Neurosci* **23**, 5503-5506.
- Steiner P., M. J. Higley, W. Xu, B. L. Czervionke, R. C. Malenka and B. L. Sabatini** (2008). "Destabilization of the postsynaptic density by PSD-95 serine 73 phosphorylation inhibits spine growth and synaptic plasticity." *Neuron* **60**(5), 788-802.
- Stoppini L., P. A. Buchs and D. Muller** (1991). "A simple method for organotypic cultures of nervous tissue." *J Neurosci Methods* **37**(2), 173-82.
- Sturgill J. F., P. Steiner, B. L. Czervionke and B. L. Sabatini** (2009). "Distinct domains within PSD-95 mediate synaptic incorporation, stabilization, and activity-dependent trafficking." *J Neurosci* **29**(41), 12845-54.
- Svoboda K. and R. Yasuda** (2006). "Principles of two-photon excitation microscopy and its applications to neuroscience." *Neuron* **50**(6), 823-39.

- Takumi Y., V. Ramirez-Leon, P. Laake, E. Rinvik and O. P. Ottersen** (1999). "Different modes of expression of AMPA and NMDA receptors in hippocampal synapses." *Nat Neurosci* **2**(7), 618-24.
- Tanaka J., Y. Horiike, M. Matsuzaki, T. Miyazaki, G. C. Ellis-Davies and H. Kasai** (2008). "Protein synthesis and neurotrophin-dependent structural plasticity of single dendritic spines." *Science* **319**(5870), 1683-7.
- Topinka J. R. and D. S. Bredt** (1998). "N-terminal palmitoylation of PSD-95 regulates association with cell membranes and interaction with K+ channel Kv1.4." *Neuron* **20**(1), 125-34.
- Valtschanoff J. G. and R. J. Weinberg** (2001). "Laminar Organization of the NMDA Receptor Complex within the Postsynaptic Density." *The Journal of Neuroscience* **21**(4), 1211-1217.
- Van Harrevelde A. and E. Fifkova** (1975). "Swelling of dendritic spines in the fascia dentata after stimulation of the perforant fibers as a mechanism of post-tetanic potentiation." *Exp Neurol* **49**(3), 736-49.
- Weed S. A., A. V. Karginov, D. A. Schafer, A. M. Weaver, A. W. Kinley, J. A. Cooper and J. T. Parsons** (2000). "Cortactin localization to sites of actin assembly in lamellipodia requires interactions with F-actin and the Arp2/3 complex." *J Cell Biol* **151**(1), 29-40.
- Xie Z., D. P. Srivastava, H. Photowala, L. Kai, M. E. Cahill, K. M. Woolfrey, C. Y. Shum, D. J. Surmeier and P. Penzes** (2007). "Kalirin-7 controls activity-dependent structural and functional plasticity of dendritic spines." *Neuron* **56**(4), 640-656.
- Yoshihara Y., M. De Roo and D. Muller** (2009). "Dendritic spine formation and stabilization." *Curr Opin Neurobiol*.
- Yoshii A. and M. Constantine-Paton** (2007). "BDNF induces transport of PSD-95 to dendrites through PI3K-AKT signaling after NMDA receptor activation." *Nat Neurosci* **10**(6), 702-11.
- Yoshii A., Y. Murata, J. Kim, C. Zhang, K. M. Shokat and M. Constantine-Paton** (2011). "TrkB and Protein Kinase M {zeta} Regulate Synaptic Localization of PSD-95 in Developing Cortex." *J Neurosci* **31**(33), 11894-904.
- Yuste R. and T. Bonhoeffer** (2001). "Morphological changes in dendritic spines associated with long-term synaptic plasticity." *Annu Rev Neurosci* **24**, 1071-89.
- Yuste R. and T. Bonhoeffer** (2004). "Genesis of dendritic spines: insights from ultrastructural and imaging studies." *Nat Rev Neurosci* **5**(1), 24-34.

Zhang P. and J. E. Lisman (2011). "Activity-dependent regulation of synaptic strength by PSD-95 in CA1 neurons." *J Neurophysiol*.

8. Acknowledgements

First of all, I want to thank Dr. Volker Scheuss for supervising my thesis and introducing me into the two-photon imaging technique. He was extremely fast when in charge of his assignment as supervisor, and his support was very helpful. Although adapting to each other was not always easy, his mentorship resulted in a highly productive and very professional collaboration with mutual understanding, and I learnt a lot from him. I wish him all the best to become a great professor.

I am very thankful to Prof. Dr. Tobias Bonhoeffer for giving me the opportunity to conduct my PhD research in his department. Although he often had an extremely busy schedule, he found the time for fruitful scientific and non-scientific discussions.

Great thank goes to my thesis committee members Oliver Griesbeck and Martin Kerschensteiner. I also want to thank Prof. Dr. Valentin Stein, Barbara Cokic and Manuel Berning for their collaboration and advice. And I thank Dr. Corette Wierenga and Prof. Dr. Daniel Choquet for providing me with DNA plasmids.

I thank the Boehringer Ingelheim Fonds (BIF) and IMPRS for funding and personal support. At this point I also want to thank Hans-Jörg Schäffer, Ingrid Wolf and Maximiliane Reif for making IMPRS possible, as well as for their advice and help.

I am very grateful to Marianne Braun and Ursula Weber from the EM facility, and to my intern Jens Stadler for help with EM data analysis. I thank them not only for their great collaboration, but also for their enthusiasm, humour and exhilarant conversations. My thanks also go to Volker Staiger, Frank Voss, Claudia Huber, Nancy Meyer, and Max Sperling for technical and experimental assistance.

A big “thank you” goes to Juliane Jäpel for reading and correcting the manuscript of my PhD thesis. She became a good colleague and friend, and we shared a great time during the “Deutsche Schülerakademie 2012”.

Greats thanks also to the entire Bonhoeffer group. You all were amazing friends!

Finally and most importantly, I would like to thank my wonderful wife Diana Zinatullina, my mother Christine Meyer, my father Ernst Meyer and my sister Jasmin Schott, for their encouragement, patience and love. I wish I would have had more time to spend with you in the last couple of years.

9. Curriculum Vitae

Personal Details

Name: Daniel Meyer

Born in Dachau on March 12th 1982

Present contact:

Gräfelfinger Straße 70c

81375 Munich

Phone: +49/89/38076455

Cell Phone: +49/176/24207025

E-mail: mail.daniel.meyer@gmail.com

Education

since 06/08

*PhD student at the Max Planck Institute of Neurobiology,
Martinsried, Germany*

Topic: " Correlated plasticity of synaptic structures and its relationship to the stabilization of synaptic enlargement"
Group of Prof. Dr. Tobias Bonhoeffer / Dr. Volker Scheuss
International Max Planck Research School (IMPRS)

09/07-02/08

Master's Thesis at Stanford University, USA (Mark: 1.3)

Topic: "Protein folding - purification und structural analysis of chaperones"

10/06-02/08

Master's Biochemistry, M.Sc. (Mark: 1.6)

Major subjects: Biochemistry and Molecular Cell Biology

Minor subject: Structural Biology

Additional voluntary minor subject: Virology

Ludwig Maximilian University Munich and Stanford University

10/05-09/06

*Master's Chemistry (without degree, transfer into Master's
Biochemistry)*

Major subjects: Inorganic and Organic Chemistry

Minor subject: Biochemistry

Ludwig Maximilian University Munich

- 06/05-09/05 Bachelor's Thesis (Mark: 1.3)
 Topic: "Kumada Cross Coupling Reactions and Synthesis of Aryl-Sulfonates"
 Ludwig Maximilian University Munich
- 10/02-09/05 Bachelor's Chemistry and Biochemistry, B.Sc. (Mark: 2.2)
 Subjects: Inorganic, Organic and Physical Chemistry,
 Biochemistry
 Ludwig Maximilian University Munich
- 09/93-06/02 European High School, Gymnasium bei St. Anna, Augsburg
(Mark: 1.7)

Practical Experience (internships outside of studies)

- 03/07-04/07 Internship Virology, HIV Research
 Julius Maximilian University Würzburg and Helmholtz Centre
 Munich
 Topic: "Functional characterization of HIV and EFV proteins"
- 08/06-09/06 Internship Stem Cell Research, Helmholtz Centre Munich
 Topic: "Stem cell research - Endoderm formation in the
 mouse"
- 07/04-08/04 Working Student at DoNatur GmbH, IZB Martinsried
 Topic: "Extraction of anti-rheumatic agents"

Publications

- Paper from PhD Thesis: in progress
- Jose H. Pereira, Corie Y. Ralston, Nicholai R. Douglas, **Daniel Meyer**, Kelly M. Knee, Daniel R. Goulet, Jonathan A. King, Judith Frydman and Paul D. Adams, "Crystal Structures of a Group II Chaperonin Reveal the Open and Closed States Associated with the Protein Folding Cycle", J. Biol. Chem. 2010, 285, 27958-27966. **Cover Article** and "**Paper of the Week**".
- Lutz Ackermann, Robert Born, Julia H. Spatz, **Daniel Meyer**, "Efficient Aryl - (Hetero-)Aryl Coupling via Activation of C-Cl and C-F Bonds Using Nickel Complexes of Air-Stable Phosphine Oxides" Angew. Chem. 2005, 117, 7382-7386; Angew. Chem. Int. Ed. 2005, 44, 7216-7219. "**Hot Paper**".

Conferences

- Scheuss, V., **Meyer, D.**, Bonhoeffer, T., Analysis of Dendritic Spine Plasticity by 2-Photon Glutamate Uncaging and 2-Photon Imaging, 8th Goettingen Meeting of The German Neuroscience Society, Goettingen, Germany, 2009.
- **Meyer, D.**, Bonhoeffer, T., Scheuss, V., Analysis of Dendritic Spine Plasticity by 2-Photon Glutamate Uncaging and 2-Photon Imaging, Interact Symposium, Munich, Germany, 2009.
- **Meyer, D.**, Scheuss, V., Bonhoeffer, T., Analysis of Dendritic Spine Plasticity by 2-Photon Glutamate Uncaging and 2-Photon Imaging, 9th Goettingen Meeting of The German Neuroscience Society, Goettingen, Germany, 2011.
- **Meyer, D.**, Bonhoeffer, T., Scheuss, V., Relationship between Structural Plasticity of Dendritic Spines and Postsynaptic Density, 8th FENS Forum of Neuroscience, Barcelona, Spain, 2012.

Scholarships

Stipend of the Boehringer Ingelheim Fonds (BIF), Stipend of the Max Planck Society, IMPRS Stipend, DAAD Stipend for Master's Thesis at Stanford University, E-fellows Stipend

Additional Skills

- Certified courses in business/economics (48 hours), project management (40 hours, LMU, mark: 1) and in marketing, sales and product management (40 hours, LMU, mark: 1)
- Strategy workshop at McKinsey & Company
- Data acquisition and data analysis with MatLab, ImageJ and Excel, Pymol, basics in HTML
- Adobe Illustrator, Adobe Photoshop, Open Project, Microsoft Office Suite
- TOEFL internet-based: 106 out of 120 points
- Various soft skill workshops (IMPRS, Boehringer Ingelheim Fonds, LMU)
- Attendance at different international conferences, symposia, retreats and seminars

Engagement

- Teaching: course instructor at the "Deutsche Schülerakademie 2012" (German Pupil Academy) and supervision / mentoring of interns
- Fundraising for a social event at the Max Planck Institutes of Biochemistry and Neurobiology
- Financial administrator within the graduate program at the Max Planck Institute of Neurobiology

- "Biotechnologische Studenteninitiative" (Bts): customer acquisition for the job fair "ScieCon2009"
- Speaker of the student dormitory (2004-2006)
- Training and commitment as volunteer firefighter (squad leader) (Auxiliary Fire Brigade Augsburg-Inningen and Munich-Großhadern, 1999-2006)

Present Languages

German (Native Language), English (fluent), French (Basics), Spanish (Basics), Russian (Basics), Latin ("großes Latinum")

